A singular perturbation problem for a fourth order ordinary differential equation

R. Kuske[1] and L.A. Peletier[2]

Abstract

In higher order model equations such as the Swift-Hohenberg equation and the nonlinear beam equation, different length scales may be distinguished, depending on the parameters in the equation. In this paper we discuss this phenomenon for stationary solutions of the Swift-Hohenberg equation and show that when the scales are very different a multi-scale analysis can be used to yield asymptotic expressions for multi-bump periodic solutions and the bifurcation diagram of such solutions with prescribed qualitative properties, such as the number of bumps.

Key words. singular perturbation, multi-scale, oscillations.

AMS subject classifications. 34B16, 34C15, 34E13, 34G15, 34J40, 47J10

1 Introduction

In this paper we study a singular perturbation problem for the fourth order ordinary differential equation

$$\varepsilon^2 u^{iv} + u'' + u + \gamma f(u) = 0. \tag{1.1}$$

Here primes denote differentiation with respect to the independent variable x, and ε and γ are positive constants. The function f will be an odd function, such that $f(s) = o(s)$ as $s \to 0$. In this paper we shall mainly focus on the function

$$f(s) = s^3. \tag{1.2}$$

This is a canonical model for steady-state patterns in fourth order systems. For instance, through a scaling of the independent variable, equation (1.1)can be transformed to the equation

$$u^{iv} + qu'' + u + \gamma f(u) = 0, \qquad q = \frac{1}{\varepsilon}, \tag{1.3}$$

which has recently been the subject of considerable interest. It arises in the context of many fourth order model equations in physics and mechanics, such as the Swift-Hohenberg equation [6], [18] and the nonlinear beam equation used to describe travelling waves in suspension bridges [11], [12],[15] and the folding of rock layers [17]. We refer to [16] and the literature cited therein.

It has been shown in [14], [16] that equations (1.3) and (1.1) have a multitude of multi-bump periodic solutions, the number of bumps increasing as $q \to \infty$ or as $\varepsilon \to 0$. It was found numerically that many of these solutions exhibit a characteristic shape: a *Base line solution* with a *high-frequency periodic solution* superimposed on it. An example of such a periodic solution is shown in Figure 1.

[1]Department of Mathematics, University of British Columbia, Vancouver, BC Canada V6T1Z2, email: rachel@math.ubc.ca

[2]Mathematical Institute, Leiden University, PB 9512, 2300 RA Leiden and Centrum voor Wiskunde en Informatica (CWI), Amsterdam, The Netherlands, email: peletier@math.leidenuniv.nl

Understanding the conditions under which these patterns are observed, and having the ability to construct their behavior is crucial in studying complex spatial behavior, as well as providing a basis for exploring temporal behavior in the full spatio-temporal model (e.g. replacing the zero on the right hand side of (1.1) by u_t in the case of Swift-Hohenberg type models, and by $-u_{tt}$ for models describing elastic behavior).

In addition to serving as a canonical model for fourth order systems, such as those listed in paragraph below equation (1.3), many of the phenomenon observed in this model are also observed in coupled second order systems. The Swift-Hohenberg equation has been used as a "toy" problem for studying pattern formation in coupled reaction-diffusion patterns [10], and localized and multi-bump patterns, which have been observed in models of elastic buckling [4], have been observed through similar mechanisms in coupled KdV-type models in optics [5]. Therefore, understanding the construction and asymptotic behavior of solutions to (1.1) opens the door for similar investigations of multi-bump patterns in these related systems.

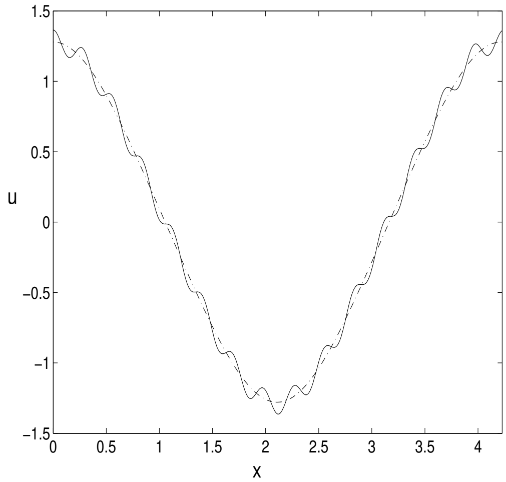

Figure 1: Numerical solution and Baseline solution for $E = 0$ and $m = 7$ (cf. (1.12))

In this paper we use a multi-scale asymptotic analysis to compute families of periodic solutions of equation (1.1) for small values of ε. In particular we consider *even* periodic solutions $u(x)$ so that

$$u'(0) = 0 \qquad \text{and} \qquad u'''(0) = 0, \tag{1.4}$$

which are *odd* with respect to some of their zeros. We denote the *smallest* value of $x > 0$, where both u and u'' vanish by $x = L$. Thus,

$$u(L) = 0 \qquad \text{and} \qquad u''(L) = 0. \tag{1.5}$$

With these conditions satisfied, the function $u(x)$, when extended appropriately over all of $\mathbf{R}$, yields a periodic solution with period $4L$.

Solutions $u(x)$ of equation (1.1) can be characterised by the data at the origin; in addition to (1.4) we set

$$u(0) = \alpha \qquad \text{and} \qquad u''(0) = \beta. \tag{1.6}$$

Throughout we shall assume that $\alpha > 0$. This involves no loss of generality since the function f is assumed to be odd.

Alternatively, one can use the value E of the first integral of equation (1.1) as a parameter: when we multiply (1.1) by u' and integrate, we find that

$$\varepsilon^2\Big\{u'u''' - \frac{1}{2}(u'')^2\Big\} + \frac{1}{2}(u')^2 + \frac{1}{2}u^2 + \gamma F(u) = E, \qquad F(u) = \int_0^u f(s)\,ds, \tag{1.7}$$

where the constant E is often referred to as the *Energy*. A relation between α, β and E is found by evaluating (1.7) at the origin. This yields

$$\varepsilon^2\beta^2 = \alpha^2 + 2\gamma F(\alpha) - 2E. \tag{1.8}$$

We shall usually characterise u by α and E, and let β be either positive or negative.

When α and E are given, and the sign of β has been fixed, then $u(x)$ is determined, so that the two conditions at $x = L$ cause the problem to be overdetermined. We find that only for discrete values of ε can both of these conditions be satisfied. The value of L then follows from the choice of α, E, and ε.

Below we state one of the main results of this paper. It identifies a sequence ε_m which tends to zero as $m \to \infty$, along which we find periodic solutions of the type described above, and it gives their asymptotic structure as $m \to \infty$.

Main result: Suppose that $f(s) = s^3$, and that

$$E = O(1) \quad \text{and} \quad \varepsilon\alpha = o(1) \qquad \text{as} \quad \varepsilon \to 0. \tag{1.9}$$

Then the leading order contribution in the asymptotic expansion for u is given by a multi-scale solution, composed of a high-frequency oscillation and a baseline solution:

$$u(x) \sim B_0(x) \pm \varepsilon\rho \cos\left(\frac{x}{\varepsilon}\right). \tag{1.10}$$

where the + sign applies when $u''(0) < 0$ and the minus sign when $u''(0) > 0$. The baseline solution $B = B(x)$ satisfies the reduced problem

$$\begin{cases} B'' + B + \gamma B^3 = 0 & \text{on} \quad (0, L), \\ B'(0) = 0, \qquad B(L) = 0. \end{cases} \tag{1.11}$$

For given α and E, this solution satisfies the symmetry conditions for values of ε such that

$$\frac{L}{\varepsilon} = (2m+1)\frac{\pi}{2}, \qquad m = 0, 1, 2, \ldots. \tag{1.12}$$

The scaled amplitude ρ of the high-frequency oscillation and that of the baseline solution are given by the initial condition

$$B(0) \sim \alpha \mp \varepsilon\rho(\alpha, E, \varepsilon), \tag{1.13}$$

in which

$$\rho(\alpha, E, \varepsilon) = \sqrt{\alpha^2 + 2\{\gamma F(\alpha) - E\}}. \tag{1.14}$$

We note that to leading order, the amplitude

$$M = \max\{|u(x)| : x \in \mathbf{R}\}$$

is given by

$$M = \begin{cases} \alpha & \text{if} \quad u''(0) < 0, \\ \alpha(1 + 2\varepsilon\rho) & \text{if} \quad u''(0) > 0. \end{cases} \tag{1.15}$$

It follows from (1.10)-(1.14) and an elementary analysis of Problem (1.11) that as $\alpha \to \infty$, the quantities M, L, m and $\rho(\alpha, E, \varepsilon)$ are related to ε and α through the following scaling relationships:

$$M = O(\alpha) \quad \text{and} \quad L = O(\alpha^{-1}) \quad \text{as} \quad \alpha \to \infty, \tag{1.16}$$

$$m = O((\varepsilon\alpha)^{-1}) \quad \text{and} \quad \rho = O(\varepsilon\alpha) \quad \text{as} \quad \varepsilon\alpha \to 0. \tag{1.17}$$

Alternatively, as $\alpha \to 0$ and in addition $E = 0$, then $\rho = O(\varepsilon)$ and $M = O(\alpha)$, and we find from (1.11) and (1.12) that

$$L \to \frac{\pi}{2} \quad \text{and hence} \quad m = O(\varepsilon^{-1}) \quad \text{as} \quad \varepsilon \to 0. \tag{1.18}$$

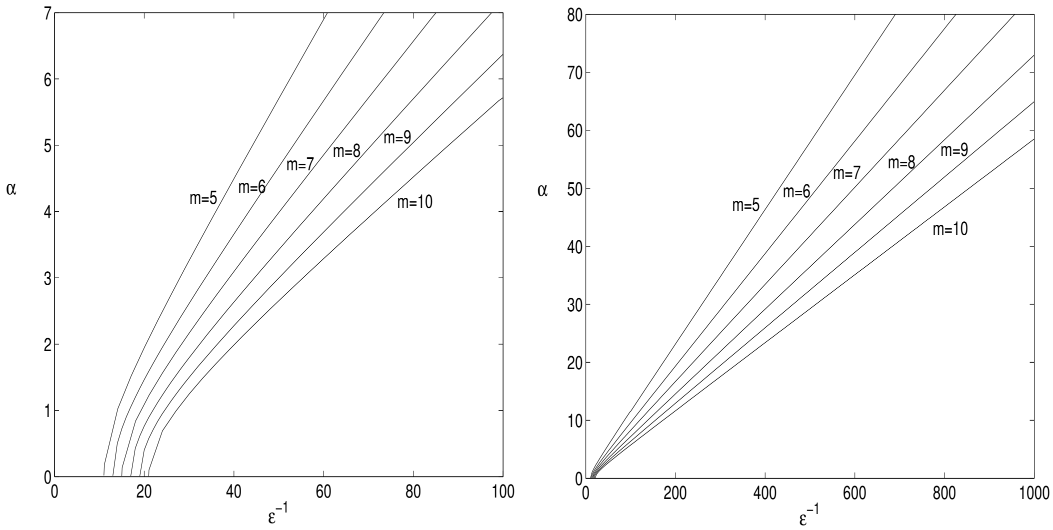

Figure 2: The curves $\mathcal{C}_m$ for $m = 5, 6, 7, 8, 9, 10$.

For each $m \geq 1$ and E fixed, equation (1.12) yields a relation between α and ε, which we can represent as a curve $\mathcal{C}_m$ in the (α, ε)-plane. If $E < 0$ and α is bounded, then, when ε is sufficiently small, solution graphs on $\mathcal{C}_m$ exhibit at least $n = 2m+1$ monotone segments – or *laps* – in a half period $(0, 2L)$. In Figure 1 we show a numerically computed solution on $\mathcal{C}_7$ when $E = 0$ which is seen to have $n = 15$ laps on $(0, 2L)$. In Figure 2 we present the bifurcation curves $\mathcal{C}_m$ for $m = 5, \ldots, 10$ and $E = 0$. With the asymptotic expression of the multi-scale solution (1.10), we can graph the solution branches corresponding to different multi-bump solutions indexed by m; for clarity we have depicted them in the $(\alpha, 1/\varepsilon)$-plane. In our analysis below, we show that these curves can be written in terms of a scaling exponent $0 < \nu < 1$, $\alpha = \varepsilon^{-\nu}$. While the curves appear to be asymptotically linear, in fact ν is increasing for the range of ε shown. On the smaller scale graph (on the left) in which $\varepsilon^{-1} \leq 100$ we find that $\nu < .55$, and on the larger scale graph (on the right) in which $\varepsilon^{-1} \leq 1000$, we find that $\nu < .7$. Although m is not particularly large here, the asymptotic results compare well with the numerical solution, as shown in Sections 3-5.

In the following sections we give the construction of the asymptotic behavior of the solutions along these branches. We show that the structure of the solution along any branch remains the same under a simple rescaling, while fixing α and varying ε corresponds to changing m and the corresponding high-frequency oscillations in the solution. We also mention here a more abstract approach to the questions discussed here that recently appeared in [2].

In Section 2 we give an outline of the multi-scale method which we employ. Then, in Section 3 we analyse the case when the energy E is $O(1)$ as $\varepsilon \to 0$. In Section 4 we give the multi-scale approximations for the case when E is large. The solution has a similar structure to the one described above, but the relative scalings are different. For example, for large E and negative, it is possible to have a solution composed of a baseline solution and high-frequency oscillations which have the same order of magnitude. In Section 5 we discuss the shape of the solutions on the curves $\mathcal{C}_m$, and in particular the number of laps. We also derive asymptotic formulae for the bifurcation graphs such as shown in Figure 2 when E is a fixed constant and α is large, and we compare these formulae with numerical results. We conclude with two appendices which give details of the computations referred to in the text.

2 Motivation

To motivate the scalings used in the following sections, we start with an intuitive asymptotic analysis of equation (1.1) in which we put $f(u) = u^3$:

$$\varepsilon^2 u^{iv} + u'' + u + \gamma u^3 = 0. \tag{2.1}$$

The naive asymptotic solution would consist of substituting the expansion

$$u(x) = \sum_{j=0}^{n} \varepsilon^j u_j(x)$$

into (2.1) and collecting like powers of ε. Then the leading order term $u_0(x)$ satisfies the equation

$$u_0'' + u_0 + \gamma u_0^3 = 0. \tag{2.2}$$

However, it is evident that in general we cannot find a solution of this equation which satisfies all the boundary conditions at $x = 0$ and $x = L$, even if we do not a-priori fix L. This is typical of a singular perturbation problem, in which the highest order derivative is neglected to leading order in the naive asymptotic approximation.

To obtain a solution of (2.1) which satisfies the complete set of boundary conditions we need to incorporate the fourth order term u^{iv} into the leading order term of the expansion. To achieve this, we introduce a scaling of the independent variable so that the first two terms in (2.1) become of equal order. Introducing the variables

$$\xi = \varepsilon^{-s} x \qquad \text{and} \qquad U(\xi) = u(x), \qquad s > 0 \tag{2.3}$$

into (2.1) yields

$$\varepsilon^{2(1-2s)} U^{iv} + \varepsilon^{-2s} U'' + U + \gamma U^3 = 0. \tag{2.4}$$

To balance the derivative terms in the leading order equation for U, we set $s = 1$. This yields the equation

$$U^{iv} + U'' = 0 \tag{2.5}$$

with the general solution

$$U = A\cos\xi + C\sin\xi + B,$$

in which A, B, and C are constants.

In order to combine aspects of both the naive expansion and the singular perturbation expansion, one recognizes that the solution must depend on two scales: a *fast* scale ξ and the *slow* scale x. Even though ξ is defined in terms of x, in the formal multi-scale analysis these two scales are treated as independent variables. That is, functions of x are treated as constants compared to the rapidly varying functions of ξ.

The observation that u depends on two spatial scales, ξ and x, suggests that the solution can be written in a more general way, that is,

$$u(x) = U(x,\xi) + w(x) + y(\xi). \tag{2.6}$$

Without loss of generality we can absorb $y(\xi)$ into $U(x,\xi)$. Then, treating ξ and x as independent variables, in the spirit of multi-scale analysis [7], we obtain for $u' = u'(x)$:

$$u' = U_x + \frac{1}{\varepsilon}U_\xi + w_x. \tag{2.7}$$

Higher order derivatives of $u(x)$ are written in a similar manner. Upon substituting these derivatives into (2.1), expanding the function $U(x,\xi)$ in a power series of ε

$$U(x,\xi) = \sum_{j=0}^{n} \varepsilon^j U_j(x,\xi),$$

and equating the coefficients of equal powers of ε to zero, we obtain the following sequence of equations:

$$\begin{aligned}
&(2.8) \qquad && O(\varepsilon^{-2}) \qquad && U_{0\xi\xi\xi\xi} + U_{0\xi\xi} = 0,\\
& && O(\varepsilon^{-1}) \qquad && U_{1\xi\xi\xi\xi} + U_{1\xi\xi} = -4U_{0x\xi\xi\xi} - 2U_{0x\xi} = 0,\\
&(2.9) \qquad && O(1) \qquad && w_{xx} + w + \gamma w^3 = 0.
\end{aligned}$$

The derivation of these equations has been included in Appendix A.

Note that this sequence of equations includes equations of the form obtained from the naive expansion (compare (2.9) and (2.2)), as well as equations obtained from the introduction of the fast variable ξ (compare (2.8) and (2.5)). In fact, as we show later, the solution of (2.9) yields the *baseline solution* mentioned in the introduction, and by solving for U we obtain the multi-scale behavior of the *high-frequency periodic solution*.

The solution of (2.8) is given by

$$U_0(x,\xi) = A(x)\cos\xi + C(x)\sin\xi + \tilde{B}(x), \tag{2.10}$$

in which the coefficients $A(x)$ and $C(x)$, and $\tilde{B}(x)$ are treated as constants with respect to ξ. Note that the term $w(x)$ in (2.5) can be combined with $\tilde{B}(x)$ into a single function

$B(x)$, so that the leading order behavior of the solution $u(x)$ of (2.1) is given by (2.10), i.e.

$$u(x) \sim A(x)\cos\xi + C(x)\sin\xi + B(x). \tag{2.11}$$

This gives the basic structure of the solution, with $B(x)$ determined from (2.9) and the "slowly varying" coefficients A and C, together with corrections to the frequency, given through a detailed multi-scale expansion which includes the boundary conditions and higher order terms.

Later we show that the analysis is naturally divided into cases related to the order of magnitude of the energy. For $E = O(1)$ and $M = O(1)$ as $\varepsilon \to 0$ we find that the *baseline* solution $B(x)$ is $O(1)$ and that the envelope of the *high-frequency periodic solution* given by $A(x)$ and $C(x)$ is $O(\varepsilon)$ or smaller. That is, the solution is characterized by a larger oscillation on the slow scale, with superimposed fast oscillations which are an order of magnitude smaller. This follows from a straightforward multi-scale analysis with (2.11) as the starting point. In Figure 1 we have shown a solution of this type. The general form of the solution for $E = O(1)$ is given as the Main Result in the Introduction, and constructed in detail in Section 3.

Large solutions

In order to track the bifurcation branches in Figure 2 for larger values of M, we consider a more general scaling and put $\alpha = \varepsilon^{-\nu}$, in which $\nu > 0$. We outline the rescaling and balancing of terms, which is somewhat more complicated than the balancing of terms given above. It is important to note that we allow a general scaling of several important parameters (L, α, and E), but by tracking the multi-scale behavior we are led to scaling relationships which can all be expressed in terms of a single scaling exponent.

We begin by scaling the solutions by a factor $\varepsilon^{-\nu}$, where $\nu > 0$, and by introducing a new length scale involving a factor $\varepsilon^{-\theta}$ in which $\theta > 0$ is as yet undetermined. Thus, we set

$$\varepsilon^{\nu} u(x) = v(z) \qquad \text{and} \qquad \varepsilon^{\theta} z = x. \tag{2.12}$$

We also introduce a scaling for the yet unknown length L which is $L = \varepsilon^{r} L_0$, where $L_0 = O(1)$. This leads to the following equation:

$$\varepsilon^{2k} v_{zzzz} + \varepsilon^{2\ell} v_{zz} + \varepsilon^{2\nu} v + \gamma v^3 = 0 \tag{2.13}$$

in which k and ℓ are defined by

$$k = 1 + \nu - 2\theta \qquad \text{and} \qquad \ell = \nu - \theta. \tag{2.14}$$

Our goal will be to determine r and θ in terms of ν by looking for solutions v which have a multi-scale structure similar to the one described above in (2.11). In order to construct such a solution it will be necessary to choose $k > \ell$.

The high-frequency oscillations are described by balancing the first two terms in (2.13) in terms of a suitably chosen *fast* variable $\xi = \varepsilon^{\ell - k} z$, where we have chosen $k - \ell > 0$. Then the baseline solution is determined by balancing the last three terms in terms of the *slow* variable (z). Without loss of generality we set $\theta = \nu$ so that $\ell = 0$. Then the baseline solution is $O(1)$ in the variable z; choosing $\ell \neq 0$ would eventually lead to an additional rescaling of both the baseline solution and the spatial variable, which would be equivalent to setting $\nu = \theta$. From (2.14) we conclude that $k = 1 - \nu$. Since $k > \ell = 0$, this implies that $1 - \nu > 0$. Thus, the slow and the fast variable become

$$z = \frac{x}{\varepsilon^\nu} \qquad \text{and} \qquad \xi = \frac{z}{\varepsilon^{1-\nu}} = \frac{x}{\varepsilon}, \tag{2.15}$$

where the following assumptions have been made about the exponent ν:

$$0 < \nu < 1. \tag{2.16}$$

Remark, Since $\ell = 0$, the singular perturbation term in equation (2.13) is now $\varepsilon^{2k} v^{iv}$. We can write this as $\delta^2 v^{iv}$, where

$$\delta = \varepsilon^k = \varepsilon^{1-\nu} = \varepsilon\alpha.$$

As before, we can now write v in the multi-scale form

$$v(x, z) = W\left(\frac{x}{\varepsilon}, z\right) + B(z), \tag{2.17}$$

similar to (2.11), and we shall find that

$$W\left(\frac{x}{\varepsilon}, z\right) \sim \rho \cos\left(\frac{x}{\varepsilon}\right),$$

where ρ is a constant. The application of the boundary condition at $x = L$, yields

$$\cos\left(\frac{L}{\varepsilon}\right) = 0 \qquad \Rightarrow \qquad \varepsilon^{r-1} L_0 = (2m+1)\frac{\pi}{2}. \tag{2.18}$$

When $x = L$ we have $z = \varepsilon^{-\nu} L = \varepsilon^{r-\nu} L_0$, so that we require that

$$B(\varepsilon^{r-\nu} L_0) = 0. \tag{2.19}$$

For the baseline solution $B(z)$ to be $O(1)$ with respect to ε we must choose the argument $\varepsilon^{r-\nu} L_0$ in (2.19) to be $O(1)$ as well. Since $L_0 = O(1)$, this means that we must put $r = \theta = \nu$. Equation (2.18) then yields for large m,

$$m = O(\varepsilon^{\nu-1}) \qquad \text{as} \quad \varepsilon \to 0.$$

At this point we have established that the correct scalings for u, the spatial variable x, and the length L are all ε^ν. However, we have not specified ν yet. Note that specifying ν is equivalent to specifying the relationship between α and ε, which varies along each of the solution branches shown in Figure 2. In Section 3.2 we use these scalings together with the boundary and initial conditions to determine the relationship between α, E, ε and m. Thus we obtain the multi-scale solution and, in Section 5, the corresponding bifurcation branches.

Finally, we note that for the more general nonlinearity $f(u) = |u|^{p-1}u$, in which $p > 1$, the above analysis can also be carried out. We then find equation (2.13) again, with $\ell = 0$ and

$$k = 1 - \frac{p-1}{2}\nu \qquad \text{and} \qquad 0 < \nu < \frac{2}{p-1}.$$

3 The multi-scale expansion: $E = O(1)$

As discussed in the previous sections, once we have determined the correct scalings, we can proceed to look for an asymptotic approximation in the form of a multi-scale expansion. As seen in Section 2, for large solutions a preliminary rescaling by a factor $\alpha = \varepsilon^{-\nu}$ and a scaling of the spatial scale are necessary; otherwise the procedure for $O(1)$ solutions and large solutions is essentially the same. In this section we demonstrate the multi-scale expansion for both $O(1)$ and large $O(\alpha)$ solutions. For the sake of clarity, we first consider here the case when the amplitude $M = O(1)$ with respect to ε. This corresponds to $\alpha = O(1)$, as follows from (1.15).

3.1 $M = O(1)$ solutions

The result:

Below we show that for given $\alpha = O(1)$, and $E = O(1)$, the leading order asymptotic approximation to the solution $u(x)$ is

$$u(x) = B_0(x) \pm \varepsilon\sqrt{\alpha^2 + 2\gamma F(\alpha) - 2E}\,\cos\Big(\frac{x}{\varepsilon}\Big) + O(\varepsilon^2) \qquad \text{as} \quad \varepsilon \to 0, \tag{3.1}$$

where the + sign applies when $u''(0) < 0$ and the $-$ sign when $u''(0) > 0$. The baseline solution B_0 in equation (3.1) is the solution of the initial value problem

$$\begin{cases} B_0'' + B_0 + \gamma B_0^3 = 0, \\ B_0(0) = \alpha \mp \varepsilon\sqrt{\alpha^2 + 2\gamma F(\alpha) - 2E} \qquad \text{and} \quad B_0'(0) = 0. \end{cases} \tag{3.2}$$

Denoting the first zero of B_0 by L, we find that there are specific values of α and ε for which the symmetry conditions (1.5) at $x = L$ are satisfied. They are given by:

$$L = \varepsilon(2m+1)\frac{\pi}{2} \qquad m = 0, 1, 2, \dots, \tag{3.3}$$

where L depends on α and ε through (3.2).

The construction:

Using the method of multiple scales [7], we construct the asymptotic approximation to the solution as a function of both the slow (original) scale x and the fast scale $\xi = x/\varepsilon$. We assume a solution of the form

$$u(x) = U(x,\xi) + B(x) \tag{3.4}$$
$$U(x,\xi) = U_0(x,\xi) + \varepsilon U_1(x,\xi) + \dots \tag{3.5}$$
$$B(x) = B_0(x) + \varepsilon B_1(x) + \dots \tag{3.6}$$

so that $u' = U_x + \varepsilon^{-1}U_\xi + B'(x)$. From the assumption that $E = O(1)$ with respect to ε, it follows that $U_0 = 0$, that is $U = O(\varepsilon)$, as demonstrated in detail from the general multi-scale expansion presented in Appendix A. This observation introduces some simplification in the expansion. We give a brief heuristic argument for it here.

Consider the initial conditions (1.6)

$$u(0) = \alpha = U(0,0) + B(0) \tag{3.7}$$
$$u''(0) = \beta = B''(0) + \frac{1}{\varepsilon^2}U_{\xi\xi}(0,0) + \frac{2}{\varepsilon}U_{x\xi}(0,0) + U_{xx}(0,0) \tag{3.8}$$

and the equation (1.8) for E. Assuming that B and U and their derivatives are $O(1)$ or smaller at $x = 0$, and $\beta = O(\varepsilon^{-1})$ by (1.8), we arrive at the conclusion that $U_{\xi\xi} = O(\varepsilon)$. In Section 2 we showed that to leading order, $U(x, \xi) \sim A(x)\cos(\xi)$, which implies that $A = O(\varepsilon)$ and $U_0(x) \equiv 0$.

Thus, the leading order term in $U(x, \xi)$ is $\varepsilon U_1(x, \xi)$. We substitute (3.4)-(3.6) into equation (1.1) and collect the coefficients of ε^j for $j = -1, 0, 1, \ldots$. We start by considering the leading order equation,

$$O(\varepsilon^{-1}) \quad : \quad U_{1\xi\xi\xi\xi} + U_{1\xi\xi} = 0. \tag{3.9}$$

From this equation we conclude that U_1 has the form

$$U_1(x, \xi) = A_1(x)\cos\xi + C_1(x)\sin\xi + D(x)\xi + E(x). \tag{3.10}$$

By symmetry $D(x) = 0$, and $E(x)$ can absorbed into $B(x)$. This leading order result suggests a more efficient form of the expansion for $U(x, \xi)$:

$$\begin{cases} U(x, \xi) = A(x)\cos(\lambda\xi) + C(x)\sin(\lambda\xi), \\ A(x) = \varepsilon A_1(x) + \varepsilon^2 A_2(x) + \ldots \\ C(x) = \varepsilon C_1(x) + \varepsilon^2 C_2(x) + \ldots \\ \lambda = 1 + \varepsilon\lambda_1 + \varepsilon^2\lambda_2 + \ldots \end{cases} \tag{3.11}$$

In Appendix A the general expansion for U also includes higher modes such as $\cos(j\lambda\xi)$ for $j = 1, 2, 3, \ldots$. These terms are not necessary for the leading order approximation in this case, so that we have not included them here.

Substituting (3.11) into equation (1.1), we obtain the $O(1)$ equation,

$$\begin{aligned} O(1) \quad : \quad & B_0''(x) + B_0(x) + \gamma f(B_0(x)) = \\ & -2\left(\lambda_1 A_1\cos(\lambda\xi) + \lambda_1 C_1\sin(\lambda\xi) + A_1'(x)\sin(\lambda\xi) - C_1'(x)\cos(\lambda\xi)\right). \end{aligned} \tag{3.12}$$

Following the multi-scale assumption, we treat ξ and x as independent variables, which gives the following equations for B_0, A_1, and C_1:

$$B_0''(x) + B_0(x) + \gamma f(B_0(x)) = 0, \tag{3.13}$$

and

$$C_1'(x) = \lambda_1 A_1(x), \qquad A_1'(x) = -\lambda_1 C_1(x). \tag{3.14}$$

From (3.14) we conclude that

$$A_1(x) = \rho_1\cos(\lambda_1 x) \quad \text{and} \quad C_1(x) = \rho_1\sin(\lambda_1 x), \tag{3.15}$$

where ρ_1 is a constant. Note that this yields

$$U_1(x, \xi) = \rho_1\cos\Big(\frac{x}{\varepsilon} + \lambda_1 x + \ldots - \lambda_1 x\Big), \tag{3.16}$$

so that λ_1 cancels from the expression for $U_1(x, \xi)$. This is not surprising, since variation of the solution on the scale of $\varepsilon\lambda_1\xi$ is variation on the x scale, which is already captured in the coefficients A_j and C_j. Therefore, including λ_1 in the expansion yields no additional information about the solution. Thus, without loss of generality we may put $\lambda_1 = 0$, and hence set

$$A_1(x) = \rho_1 \qquad \text{and} \qquad C_1(x) = 0, \tag{3.17}$$

where ρ_1 is a constant that is yet to be determined.

Combining (3.15) and (3.17) with the boundary conditions,

$$O(\varepsilon^{-2}) \;:\; C_1(0) = 0 \tag{3.18}$$

$$O(\varepsilon^{-1}) \;:\; C_2(0) + 3A_1'(0) = 0 \tag{3.19}$$

$$A_1(L)\cos\left(\frac{L}{\varepsilon}\right) + C_1(L)\sin\left(\frac{L}{\varepsilon}\right) = 0,$$

we conclude that

$$C_2(0) = 0 \quad \text{and} \quad \cos\left(\frac{L}{\varepsilon}\right) = 0, \tag{3.20}$$

which leads to the condition (3.3) on α, ε and m.

To determine $B_0(x)$ we consider the $O(1)$ boundary conditions,

$$\begin{aligned} O(1): \quad & B_0'(0) = 0, \quad B_0(L) = 0, \\ & B_0'''(0) - C_3(0) - 3A_2'(0) = 0, \\ & A_2(L)\cos\left(\frac{\lambda L}{\varepsilon}\right) + C_2(L)\sin\left(\frac{\lambda L}{\varepsilon}\right) = 0. \end{aligned} \tag{3.21}$$

Here we have used (3.13) to conclude that $B_0''(L) = 0$. Thus $B_0(x)$ satisfies the boundary value problem which consists of (3.13) and the boundary conditions (3.21). The conditions involving A_2, C_2 and C_3 can be used to determine higher order corrections to the high frequency oscillation. We do not compute these terms here.

In order to obtain the uniform asymptotic approximation up to $O(\varepsilon^2)$, we must also consider the equation and boundary conditions at $O(\varepsilon)$. This yields B_1, the first order correction to $B_0(x)$. In Appendix A we show that $B_1 = 0$.

Thus, summarising we have found to first order:

$$u(x) = B_0(x) + \varepsilon\rho_1\cos\left(\frac{x}{\varepsilon}\right) + O(\varepsilon^2) \qquad \text{as} \quad \varepsilon \to 0. \tag{3.22}$$

At this point $B_0(x)$ and ρ_1 have not yet been determined. We find them from the initial conditions (1.6). From (3.22) we find that

$$\begin{cases} u(0) = \alpha = B_0(0) + \varepsilon\rho_1 \\ u''(0) = \beta = B_0''(0) - \dfrac{\rho_1}{\varepsilon}. \end{cases} \tag{3.23}$$

By (1.8) we have

$$\beta = \pm\frac{1}{\varepsilon}\sqrt{\alpha^2 + 2\gamma F(\alpha) - 2E}. \tag{3.24}$$

Hence, we conclude that

$$B_0(0) = \alpha - \varepsilon\rho_1(\alpha, E) \qquad \text{and} \qquad \rho_1(\alpha, E) = \mp\sqrt{\alpha^2 + 2\gamma F(\alpha) - 2E}, \tag{3.25}$$

where we have omitted the term involving $B_0''(0)$ since it is of higher order. With $B_0(0)$ determined, so is $B_0(x)$, and the proof of the result stated at the beginning of this section is complete.

Remark. Here the $O(\varepsilon)$ correction to the baseline solution B_0 is obtained by keeping the term $\varepsilon\rho_1$ in the equation (3.23) for $B_0(0)$. If the term $\varepsilon\rho_1$ is not included in the equation for $B_0(0)$, then the boundary conditions for B_1 in Problem (A.28) in Appendix A, are no longer homogeneous, and $B_1(x) \neq 0$.

3.2 Large solutions: $M \to \infty$

In this part we make essential use of the cubic growth of the nonlinearity, and throughout we put

$$f(s) = s^3 \qquad \text{as} \qquad s \to \infty. \tag{3.26}$$

As we saw in Section 2, the small parameter will now be $\delta = \varepsilon\alpha = \varepsilon^{1-\nu}$, rather than ε.

The result:

Let $E = O(1)$. Then the leading order asymptotic approximation to the solution $u(x)$ is given by

$$u(x) = \alpha \left\{ B_0(\alpha x) \pm \delta\, \rho(\alpha, E) \cos\!\left(\frac{x}{\varepsilon}\right) + O(\delta^2) \right\} \qquad \text{as } \delta \to 0, \tag{3.27}$$

where

$$\rho(\alpha, E) = \sqrt{\frac{\gamma}{2} + \frac{1}{\alpha^2} - \frac{2E}{\alpha^4}}, \tag{3.28}$$

so that

$$\rho(\alpha, E) = \sqrt{\frac{\gamma}{2}}\,[1 + O(\alpha^{-2})] \qquad \text{as } \alpha \to \infty. \tag{3.29}$$

Here the $+$ sign applies when $u''(0) < 0$ and the $-$ sign when $u''(0) > 0$. The baseline solution $B_0(z)$ is the solution of the initial value problem

$$\begin{cases} B_0'' + \alpha^{-2} B_0 + \gamma B_0^3 = 0, \\ B_0(0) = 1 \mp \delta\, \rho(\alpha, E) \quad \text{and} \quad B_0'(0) = 0. \end{cases} \tag{3.30}$$

Remark. Note that here we have defined B_0 and ρ differently, having factored out the initial value α.

Denoting the first zero of B_0 by $L_0 = \alpha L$, there are specific values of ε given by (3.3) for which the solution satisfies the symmetry conditions (1.5) at $x = L$.

In Figure 3 we show the multi-bump solution for $m = 10$ and $E = 0$ for two different values of α. Although the two solutions appear to be very similar, note the different scales on the axes of the figures. This is a striking illustration of the scaling of the solution u and the spatial variable x, which is a vital part of the construction of the asymptotic solution, as shown below. Note also the excellent agreement between the asymptotic approximation

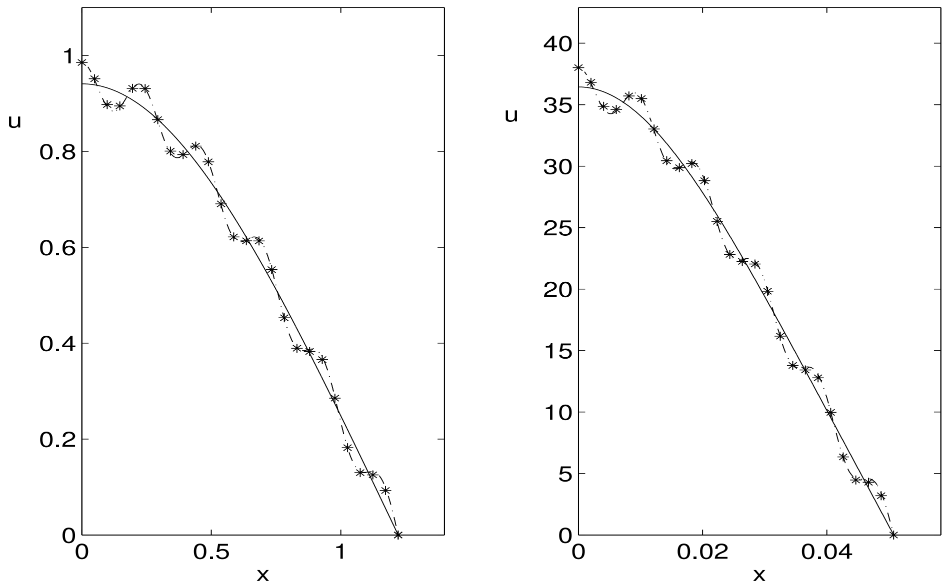

Figure 3: Solution graphs on $\mathcal{C}_{10}$ for different values of α

(the dash–dotted line) and the numerical result (the $*$'s). The solid line gives the base-line solution.

The construction:

We use the scalings given in Section 2, writing $\alpha = \varepsilon^{-\nu}$:

$$u(x) = \alpha v(z), \qquad z = \alpha x. \tag{3.31}$$

Then $L = \alpha^{-1} L_0$, and v satisfies the equation

$$\delta^2 v_{zzzz} + v_{zz} + \alpha^{-2} v + \gamma v^3 = 0, \qquad \delta = \varepsilon\alpha \tag{3.32}$$

$$v'(0) = 0, \qquad v'''(0) = 0 \tag{3.33}$$

$$v(L_0) = 0, \qquad v''(L_0) = 0 \tag{3.34}$$

where $L_0 = \alpha L$ is the first zero of $v(z)$.

The advantage of this scaling is that the resulting problem for $v(z)$ is essentially the same as the one obtained from the original problem for $u(x)$, with δ (rather than ε) as the important small parameter in the multi-scale expansion. Indeed, since by assumption $\delta \to 0$ we can find multi-scale solutions of the form,

$$v\Big(z, \frac{z}{\delta}\Big) = B(z) + W\Big(\frac{z}{\delta}, z\Big), \tag{3.35}$$

One difference in (3.32) is the coefficient α^{-2} in front of the linear term, which arises because of the different scaling. This factor plays a quantitative role in the baseline solution, but it does not affect the overall structure of the multi-scale solution.

The leading order term $B_0(z)$ in the baseline solution satisfies

$$B_0'' + \alpha^{-2} B_0 + \gamma B_0^3 = 0, \tag{3.36}$$

in which we have retained the linear term with the coefficient α^{-2} in the leading order equation for the baseline solution. Recalling that $\alpha = \varepsilon^{-\nu}$, a two-parameter perturbation expansion in both ε and δ shows that for $\nu > \frac{1}{2}$ this contribution is necessary to complete the leading order approximation, while for $\nu < \frac{1}{2}$ this contribution is not necessary, but it does not alter the leading order behavior of $v(z)$.

Thanks to the symmetry conditions, we find that the high-frequency oscillations are given by

$$W\Big(\frac{z}{\delta}, z\Big) \sim \delta\rho_1 \cos\Big(\frac{z}{\delta}\Big), \tag{3.37}$$

so that to leading order we now obtain

$$v(z) = B_0(z) + \delta\rho_1 \cos\Big(\frac{z}{\delta}\Big). \tag{3.38}$$

where ρ_1 is a constant yet to be determined.

Applying the boundary conditions yields for the baseline solution,

$$B_0'(0) = 0 \qquad \text{and} \qquad B(L_0) = 0. \tag{3.39}$$

For the high-frequency oscillation we require that

$$\cos\left(\frac{L_0}{\delta}\right) = 0 \quad \Rightarrow \quad \frac{L_0}{\delta} = (2m+1)\frac{\pi}{2}, \tag{3.40}$$

which is equivalent to (3.3).

As in Part 3.1, we determine B_0 and ρ_1 by means of the initial conditions (1.6). In view of the scaling (3.31), they yield the following initial conditions for v:

$$v(0) = 1 \qquad \text{and} \qquad v''(0) = \alpha^{-3}\beta. \tag{3.41}$$

From (3.38) we then find that

$$B_0(0) + \delta\rho_1 = 1 \qquad \text{and} \qquad -\frac{\rho_1}{\delta} = \frac{\beta}{\alpha^3}. \tag{3.42}$$

Since, by the energy identity, β is given by

$$\beta = \pm\frac{\alpha^2}{\varepsilon}\sqrt{\frac{\gamma}{2} + \frac{1}{\alpha^2} - \frac{2E}{\alpha^4}},$$

we obtain for ρ_1:

$$\rho_1(\alpha, E) = \mp\sqrt{\frac{\gamma}{2} + \frac{1}{\alpha^2} - \frac{2E}{\alpha^4}}. \tag{3.43}$$

The value of $B_0(0)$ then follows from (3.42). Since $B_0'(0) = 0$, this determines $B_0(z)$, and hence L_0, uniquely.

4 The multi-scale expansion when $|E| \to \infty$

In this section we obtain multi-scale expansions when the energy E is no longer bounded, but tends to either $+\infty$ or $-\infty$. Of course, at all times the energy identity (1.8) requires that

$$E \le \frac{1}{2}\alpha^2 + \gamma F(\alpha). \tag{4.1}$$

In Section 3 we found that when E is bounded, the amplitude of the high-frequency oscillation is small compared to that of the baseline oscillation. We shall find that when E is allowed to grow, this need no longer be true and the two amplitudes may become comparable in size.

In Figure 4 we show four solution graphs, each with the same initial value: $\alpha = 1$. In the top two $E = 0$ and ε takes on two values. In the bottom two, $E = -50$, and ε has the same values. Shown are: the asymptotic solution (dash-dotted) and the numerical solution of the original equation (1.1) (circles). We see that when we decrease ε, from $\varepsilon = 0.1$ to $\varepsilon = 0.03$ (increase $q = 1/\varepsilon$ from 10 to 33.33...), the value of m increases and the amplitude of the high-frequency oscillation decreases, as predicted by the asymptotic analysis. Thus, going from Figure 4a to Figure 4b, we hop from $\mathcal{C}_4$ to $\mathcal{C}_{12}$, and going from Figure 4c to Figure 4d, we move from $\mathcal{C}_3$ to $\mathcal{C}_{11}$. Note that the magnitude of the high frequency oscillations increases with $|E|$.

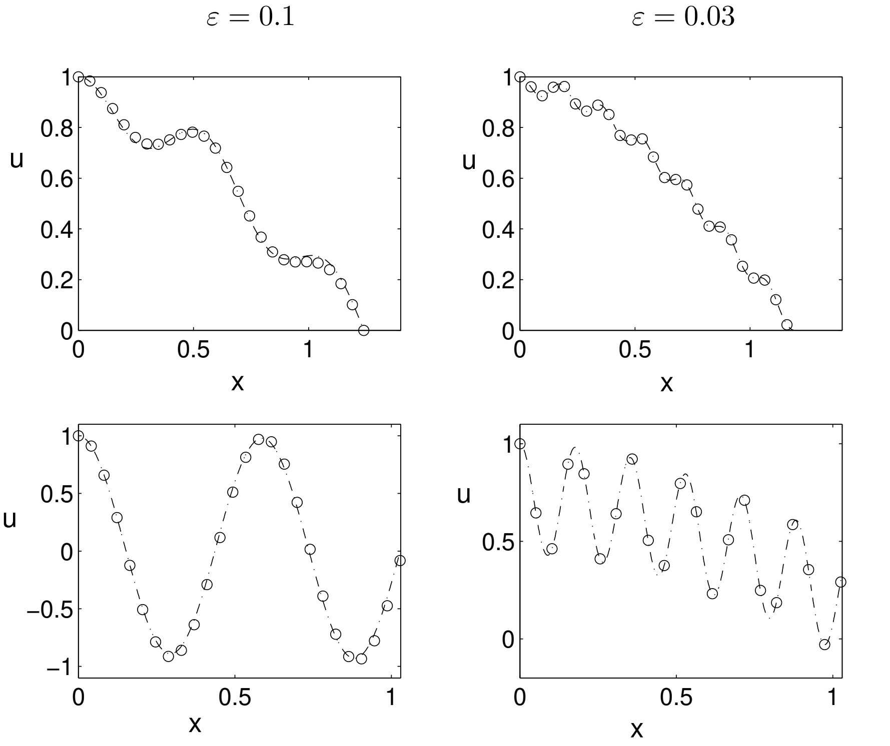

Figure 4: Solution graphs for $E = 0$ (top) and $E = -50$ (bottom), and $u(0) = 1$

4.1 $M = O(1)$ solutions

As we have seen in the previous sections, when $M = O(1)$, then so is α. Therefore, (4.1) implies that if $|E|$ is to grow to infinity, then necessarily $E \to -\infty$.

The result:

Suppose that $\alpha = O(1)$ is given, and that

$$E \sim -\frac{e_0}{\varepsilon^2} \qquad \text{as} \qquad \varepsilon \to 0, \tag{4.2}$$

where e_0 is some positive $O(1)$ constant. Then the leading order asymptotic approximation to the solution $u(x)$ is given by

$$u(x) \sim B_0(x) \pm \rho_0 \cos\Big(\frac{x}{\varepsilon}\Big), \qquad \rho_0 = \sqrt{2e_0}, \tag{4.3}$$

where $B_0(x)$ is the solution of the problem

$$\begin{cases} B_0'' + KB_0 + \gamma f(B_0) = 0, & K = 1 + \dfrac{3}{2}\gamma\rho_0^2, \\ B_0(0) = \alpha \mp \rho_0 \qquad \text{and} & B_0'(0) = 0. \end{cases} \tag{4.4}$$

Note that in contrast to the case $E = O(1)$, the amplitude ρ_0 of the high-frequency solution is now also $O(1)$ and plays a role in both the equation and the initial condition for $B_0(x)$. For $|E| > O(\varepsilon^{-2})$ the solutions are no longer $O(1)$, as we show in Section 4.2.

As in the earlier cases, we denote the first positive zero of B_0 by L. The symmetry conditions (1.5) at $x = L$ are then satisfied if we put

$$\frac{L}{\varepsilon} = (2m+1)\frac{\pi}{2}, \qquad m = 0, 1, 2, \ldots. \tag{4.5}$$

The construction:

We follow the procedure of Section 3.1. However, in the present case we find from (1.8) and (4.2) that

$$\beta^2 \sim \frac{2e_0}{\varepsilon^4} \qquad \text{as} \qquad \varepsilon \to 0. \tag{4.6}$$

Thus, $\beta = O(\varepsilon^{-2})$. Recall that when E is bounded, then $\beta = O(\varepsilon^{-1})$. Reconsidering (3.4) – (3.6), we find that this implies that $U_0(x) \not\equiv 0$. As is shown in Appendix A, this adds a complication to the analysis, and higher order harmonic terms involving $\cos(jx/\varepsilon)$, $j = 2, 3, \ldots$ need to be included. For further details we refer to Appendix A.

4.2 Large solutions: $M \to \infty$

Here we again make essential use of the cubic growth of the function $f(s)$, and we put

$$f(s) = s^3. \tag{4.7}$$

As in Section 3.2, we scale the solution and the spatial variable, setting, $v = u/\alpha$ and $z = \alpha x$. The scaled solution $v(z)$ is then found to have a multi-scale form (3.35), its leading order asymptotic approximation being

$$u(x) = \alpha\Big\{B_0(z) \pm \rho_0 \cos\Big(\frac{z}{\delta}\Big)\Big\} + O(\delta), \tag{4.8}$$

where $\delta = \varepsilon\alpha$. The function $B_0(z)$ is the solution of the initial value problem

$$\text{(4.9)} \qquad \begin{cases} B_0'' + \Big(\alpha^{-2} + \dfrac{3}{2}\gamma\rho_0^2\Big)B_0 + \gamma B_0^3 = 0 \\ B_0(0) = 1 \mp \rho_0 \qquad \text{and} \qquad B_0'(0) = 0, \end{cases}$$

where

$$\text{(4.10)} \qquad \rho_0(\alpha, E) = \delta\sqrt{\frac{\gamma}{2} + \frac{1}{\alpha^2} - \frac{2E}{\alpha^4}} \mp \delta^2 B_0''(0).$$

At the first positive zero $z = L_0$ of $B_0(z)$ we require that

$$\text{(4.11)} \qquad \frac{L_0}{\delta} = (2m+1)\frac{\pi}{2}, \qquad m = 0, 1, 2, \ldots .$$

The construction follows Section 3.2: the initial conditions yield two equations for ρ_0 and $B_0(0)$ which are similar to (3.42).

It is in the application of the initial conditions that the large energy plays a crucial role in the balance of the terms. Note that the asymptotic expressions (4.9)-(4.10) for ρ_0 and B_0 differ from previous cases, since they are determined through the initial conditions. There is a range of values of $|E|$ which are possible, and below we give the details of the relevant cases: remembering that $\alpha = \varepsilon^{-\nu}$, we have

$$\text{(4.12)} \qquad \begin{aligned} &E = O(\varepsilon^{-2(1+\nu)}) = O(\alpha^4/\delta^2) && \text{for} \quad E < 0, \\ &E = O(\varepsilon^{-4\nu}) = O(\alpha^4) && \text{for} \quad E > 0. \end{aligned}$$

Remark 1. Periodic solutions with large negative energy arise in connection with a variational problem associated with (1.1), which involves the functional

$$J_\varepsilon(u, L) = \frac{1}{2L}\int_{-L}^{L}\Big\{\frac{\varepsilon^2}{2}(u'')^2 - \frac{1}{2}(u')^2 + F(u)\Big\}\,dx.$$

Here $2L$ denotes the period of u, and one minimises J_ε over all periodic solutions where the period is also allowed to vary. Then there exists a minimiser u^*, with period L^* [9]. The minimiser u^* and its half period L^* have the following properties:

$$\text{(a)} \qquad J_\varepsilon(u^*, L^*) = E(u^*),$$

in which $E(u^*)$ denotes the energy associated with u^* (see e.g. Chapter 7 of [15]), and

$$\text{(b)} \qquad \begin{cases} \limsup\limits_{\varepsilon\to 0} \varepsilon^4 J_\varepsilon(u^*, L^*) \le -\dfrac{1}{96}, \\ \liminf\limits_{\varepsilon\to 0} \varepsilon^4 J_\varepsilon(u^*, L^*) \ge -\dfrac{1}{64}. \end{cases}$$

Thus, for these minimisers, the energy E is negative and tends to $-\infty$ with a rate given by $E = O(\varepsilon^{-4})$ as $\varepsilon \to 0$. This rate is close to the one given in the first case mentioned above where $E = O(\varepsilon^{-2(1+\nu)})$. However, there it is assumed that $\nu < 1$.

Remark 2. In this connection it is interesting to apply the scaling of x and u also to the energy identity. We then obtain

$$\delta^2 \left\{ v'v''' - \frac{1}{2}(v'')^2 \right\} + \frac{1}{2}(v')^2 + \frac{1}{2}\varepsilon^{2\nu} v^2 + \frac{1}{4}v^4 = \frac{E}{\alpha^4} = E_v. \tag{4.13}$$

Hence, in terms of the scaled energy E_v the above cases become

$$\begin{aligned} E_v &= O(\delta^{-2}) && \text{for} \quad E_v < 0, \\ E_v &= O(1) && \text{for} \quad E_v > 0. \end{aligned} \tag{4.14}$$

Case 1: E < 0: We assume that $E = O(\varepsilon^{-2(1+\nu)}) = O(\alpha^4/\delta^2)$.

In this case we find that

$$\delta\sqrt{\frac{\gamma}{2} + \frac{1}{\alpha^2} - \frac{2E}{\alpha^4}} = O(1) \qquad \text{as} \qquad \delta \to 0, \tag{4.15}$$

so that in the initial condition $u''(0) = \beta$, the first term in (4.10) gives the leading order contribution to ρ_0, i.e.

$$\rho_0(\alpha, E) \sim \delta\sqrt{\frac{\gamma}{2} + \frac{1}{\alpha^2} - \frac{2E}{\alpha^4}} \qquad \text{and} \qquad B_0(0) \sim 1 - \rho_0. \tag{4.16}$$

Case 2: E > 0: We assume that $E = O(\varepsilon^{-4\nu}) = O(\alpha^4)$.

In this case the analysis of Section 3.2 holds, unless

$$\frac{E}{\alpha^4} \to \frac{\gamma}{4} \qquad \text{as} \qquad \alpha \to \infty.$$

In that case the relative growth of α and δ^{-1} plays a role in determining which terms are dominant in the initial conditions, and so supplies the leading order approximation to ρ_0, given by either or both terms on the right hand side of (4.10). For example, if

$$\frac{E}{\alpha^4} - \frac{\gamma}{4} = O(\varepsilon^{2\nu}) = O(\alpha^{-2}) \qquad \text{as} \qquad \alpha \to \infty, \tag{4.17}$$

then for the first term in (4.10) we find that

$$\delta\sqrt{\frac{\gamma}{2} + \frac{1}{\alpha^2} - \frac{2E}{\alpha^4}} = O(\delta/\alpha), \tag{4.18}$$

and plainly, the second term is $O(\delta^2)$. Then either of the terms in (4.10) gives the leading order contribution to ρ_0, depending on whether $\alpha\delta = \alpha^2\varepsilon = \varepsilon^{1-2\nu}$ tends to zero or to infinity, or, equivalently, on the value of ν in the expression $\alpha = \varepsilon^{-\nu}$. We find that

$$\nu < \frac{1}{2} \qquad \Rightarrow \qquad \rho_0 \sim \delta\sqrt{\frac{\gamma}{2} + \frac{1}{\alpha^2} - \frac{2E}{\alpha^4}}, \tag{4.19}$$

$$\nu > \frac{1}{2} \qquad \Rightarrow \qquad \rho_0 \sim \delta^2 B_0''(0) \sim -\delta^2\gamma B_0^3(0) \tag{4.20}$$

where, in the second case we have used the fact that $\rho_0 = O(\delta^2)$. When $\nu = 1/2$, both terms balance.

Note that we retain all the linear terms in the leading order equation for the baseline solution (4.9). As in Section 3.2, keeping the term $\alpha^{-2}B_0$ effectively results in a higher order contribution included in $B_0(z)$ for $\nu < \frac{1}{2}$, but it does not alter the leading order behavior of $v(z)$.

5 Branches of multi-bump periodic solutions

In Sections 3 and 4 we have constructed asymptotic expressions for even periodic solutions with multi-scale structure: a smooth baseline solution on which a high-frequency oscillation is superimposed. These solutions are all odd with respect to some of their zeros, the first positive such zero being denoted by $x = L$, i.e.

$$u(L) = 0 \qquad \text{and} \qquad u''(L) = 0.$$

Plainly, they have period $4L$.

For a fixed number of high-frequency oscillations in $[0, 4L]$ and the energy E, these solutions lie on curves in the (ε, α)-plane; the relation between α and ε being given by the expression obtained in (1.12) and (3.40):

$$\begin{aligned} &\frac{1}{\varepsilon}L(\alpha,\varepsilon) = (2m+1)\frac{\pi}{2} \qquad m = 1,2,3,\ldots \quad \text{for } \alpha = O(1) \\ &\frac{1}{\delta}L_0(\alpha,\delta) = (2m+1)\frac{\pi}{2} \qquad m = 1,2,3,\ldots \quad \text{for } \alpha = \varepsilon^{-\nu},\ 0<\nu<1 \end{aligned} \tag{5.1}$$

In Figure 5 we compare the bifurcation curves $\mathcal{C}_m$ obtained numerically (solid) with the "full" asymptotic approximation given in Sections 1, 3 and 4 (dash-dotted). In Figure 6 we compare the numerically computed curve $\mathcal{C}_m$ (solid) with the approximation obtained for large values of α and m given in (5.7) (dash-dotted). We compare these graphs on two different scales; as expected, the approximation improves with increasing m and the relative size of the error decreases with ε.

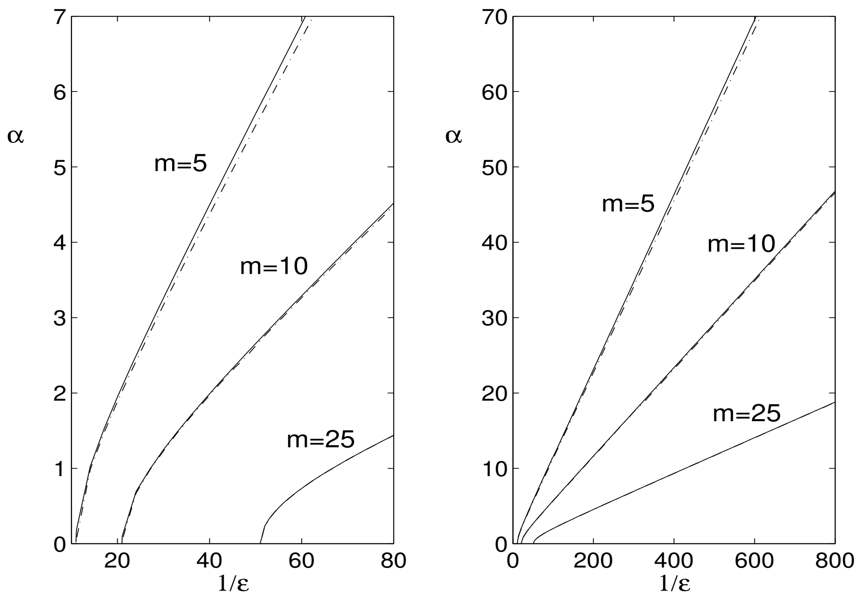

Figure 5: Bifurcation curves $\mathcal{C}_m$ for $E = 0$ for the full equation (solid) and asymptotic approximation (dash-dot)

When $E \le 0$, the integer m is closely related to the number n of monotone segments, or laps, in the graph of $u(x)$ on the half period $(0, 2L)$, and it is given by

$$n = 2m + 1.$$

To see this we inspect the sign changes of $u'(x)$. It is expedient to consider the cases $\beta < 0$ and $\beta > 0$ separately. We focus on the case when $\alpha = O(1)$ as in Section 3.

Suppose that $\beta < 0$. Then, according to (3.1),

$$u(x) = B_0(x) + \varepsilon\rho\cos\Big(\frac{x}{\varepsilon}\Big) + O(\varepsilon^2),$$

where

$$\rho = \sqrt{\alpha^2 + \frac{1}{2}\alpha^4 - 2E},$$

and hence

$$u'(x) = B_0'(x) - \rho\sin\Big(\frac{x}{\varepsilon}\Big) + O(\varepsilon).$$

In particular,

$$u'(x_k) = B_0'(x_k) - \rho + O(\varepsilon) \qquad \text{with} \qquad x_k = (4k+1)\frac{\pi}{2}\varepsilon, \qquad k = 0, 1, 2, \ldots$$

and

$$u'(y_\ell) = B_0'(y_\ell) + \rho + O(\varepsilon) \qquad \text{with} \qquad y_\ell = (4\ell+3)\frac{\pi}{2}\varepsilon, \qquad \ell = 0, 1, 2, \ldots.$$

Note that

$$x_k < y_k < x_{k+1} \qquad \text{for} \qquad k = 0, 1, 2, \ldots.$$

If $L = (2m+1)\frac{\pi}{2}\varepsilon$, then

$$\begin{aligned} &m \;\; \text{even}: \qquad k = 0, 1, 2, \ldots, \frac{1}{2}m, \qquad && L = x_{m/2} \\ &m \;\; \text{odd}: \qquad \ell = 0, 1, 2, \ldots, \frac{1}{2}(m-1), \qquad && L = y_{(m-1)/2} \end{aligned}$$

Since $B_0'(x) < 0$ for $0 < x < 2L$, it follows that $u'(x_k) < 0$ at all the points x_k contained in the interval $(0, L]$. In particular, $u'(L) < 0$.

At the points y_ℓ the situation is more delicate because the sign of $u'(y_\ell)$ depends on the balance between two positive terms. We assert that

$$u'(y_\ell) > 0 \qquad \text{for} \qquad \ell = 0, 1, 2, \ldots \frac{1}{2}(m-1).$$

In particular, this means that

$$u'(L) > 0 \qquad \text{if} \qquad m \text{ is odd}.$$

As a first observation, we note that $B_0'' < 0$ on $(0, L)$ and hence

$$u'(y_\ell) \geq B_0'(L) + \rho + O(\varepsilon).$$

Thus we only need to compare ρ with $B_0'(L)$. We compute this quantity by means of the first integral of the differential equation for B_0:

$$\big(B_0'(L)\big)^2 = B_0^2(0) + \frac{1}{2}B_0^4(0).$$

Substituting $B_0(0)$ and the expression for ρ, we obtain

$$B_0'(L) + \rho = -\{\alpha^2 + \frac{1}{2}\alpha^4\}^{1/2} + \{\alpha^2 + \frac{1}{2}\alpha^4 - 2E\}^{1/2} + O(\varepsilon).$$

Plainly, if $E < 0$, then

$$-\{\alpha^2 + \frac{1}{2}\alpha^4\}^{1/2} + \{\alpha^2 + \frac{1}{2}\alpha^4 - 2E\}^{1/2} > 0,$$

and it follows that $u'(L) > 0$ when ε is sufficiently small, as asserted.

We conclude that for ε small enough,

$$u'(x_k) < 0 \qquad \text{and} \qquad u'(y_k) > 0,$$

and hence, that u' has at least m sign changes on $(0, L)$ irrespective of whether m is even or odd. This means that the graph of $u(x)$ has at least $n = 2m + 1$ monotone segments, or laps, in the half period $(0, 2L)$.

If $\beta > 0$ the analysis is the similar and the result is the same. An asymptotic analysis as $\epsilon \to 0$ of the function $\tilde{u}$ composed of the first two terms in the expansion shows that if $E < 0$, then $\tilde{u}$ has precisely $n = 2m + 1$ laps on the interval $(0, 2L)$.

If $E > 0$ the number of laps may change along the bifurcation branches, as we see in Figure 8.

Finally, if $E = 0$ then $B_0'(L)$ and ρ balance to first order and higher order terms need to be included in the asymptotic analysis. However, for precisely this case, when $E = 0$, the existence and qualitative properties of periodic solutions with a prescribed number of laps was discussed in [3] and [15]. Specifically, it was proved that given any integer $n \geq 1$, there exists an n-lap periodic solution of equation (1.1) with $E = 0$, provided that

$$\varepsilon < \varepsilon_n = \frac{n}{n^2 + 1}, \qquad n = 1, 2, \ldots. \tag{5.2}$$

These branches of solutions were shown to bifurcate from the trivial solution $u = 0$ at points $\varepsilon = \varepsilon_n$, and approaching the axis $\{\varepsilon = 0\}$ along a vertical asymptote. Specifically, it was proved that

$$M \to \infty \qquad \text{and} \qquad M = O(1/\varepsilon) \qquad \text{as} \quad \varepsilon \to 0.$$

For the special case $n = 1$ it was established that for ε small enough,

$$\frac{1}{2\varepsilon\sqrt{2}} < M < \frac{1}{\varepsilon\sqrt{2}}.$$

5.1 Asymptotic approximation of the bifurcation curves

The relation (5.1) between α, ε and m (or n) enables us to obtain the asymptotic behaviour of these branches in the (ε, α)-plane when both m and α are large. To that end we integrate the initial value problem (3.30) for B_0 to obtain an explicit expression for $L(\alpha, \varepsilon)$. Thus we turn to the problem

$$\begin{cases} \varphi'' + \alpha^{-2}\varphi + \varphi^3 = 0, & \varphi > 0 \quad \text{on} \quad (0, \alpha L) \\ \varphi(0) = 1 \mp \delta\,\rho(\alpha, E), & \varphi'(0) = 0 \quad \text{and} \quad \varphi(\alpha L) = 0, \end{cases} \tag{5.3}$$

where we have put $\gamma = 1$. We recall that the $-$ sign in the initial value $\varphi(0)$ applies when $u''(0) < 0$, and the $+$ sign if $u''(0) > 0$. We multiply the differential equation by $2\varphi'(z)$, integrate over $(0, z)$, and use the conditions at $z = 0$, to obtain

$$(\varphi')^2 + \{\alpha^{-2}\varphi^2 + \varphi^4/2\} = \{\alpha^{-2}\varphi^2(0) + \varphi^4(0)/2\}.$$

Therefore, since $\varphi' < 0$ on $(0, \alpha L)$,

$$\varphi' = -\frac{1}{\sqrt{2}}\sqrt{\{\varphi^2(0) - \varphi^2\}\{\varphi^2(0) + \varphi^2 + 2\alpha^{-2}\}}.$$

Finally, integration of this expression over $(0, \alpha L)$, taking $\varphi = \varphi(0)\psi$, yields

$$L(\alpha, \delta) = \frac{\sqrt{2}}{1 \mp \delta\rho}\frac{1}{\alpha}\int_0^1 \frac{d\psi}{\sqrt{(1-\psi^2)\{1 + \psi^2 + 2(\alpha\varphi(0))^{-2}\}}}. \tag{5.4}$$

For $\alpha \gg 1$ and $\delta \ll 1$,

$$L(\alpha, \delta) = \frac{\sqrt{2}}{\alpha}\{\mathcal{J} + O(\delta) + O(\alpha^{-2})\}, \tag{5.5}$$

where $\mathcal{J}$ is given by

$$\begin{aligned} \mathcal{J} = \int_0^1 \frac{d\psi}{\sqrt{1-\psi^4}} &= \frac{1}{4}\int_0^\infty s^{-1/2}(1+s)^{-3/4}ds = \frac{1}{4}B\Big(\frac{1}{2}, \frac{1}{4}\Big) \\ &= \frac{\sqrt{\pi}}{4}\frac{\Gamma(1/4)}{\Gamma(3/4)} = 1.311028777\ldots. \end{aligned} \tag{5.6}$$

Here $B(x, y)$ is the Beta function and $\Gamma(x)$ the Gamma function (cf. [1]). In the evaluation of $\mathcal{J}$ we have used the transformation $\psi^4 = 1/(1+s)$.

We now use the formula (5.5) for $L(\alpha, \varepsilon)$ in (5.1) to obtain the desired asymptotic result for branches in the (ε, α)-plane:

Let E be fixed, let $n = 2m+1$ and let m be large. Then the branch of even periodic solutions which are odd with respect to two zeros per period and have n laps per half period, behaves asymptotically as

$$q = \frac{1}{\varepsilon} \sim \sqrt{2\pi}\, n\frac{\Gamma(3/4)}{\Gamma(1/4)}\alpha \qquad \text{as} \qquad \alpha \to \infty. \tag{5.7}$$

In Figure 6 we compare the asymptotic behaviour of the branches $\mathcal{C}_m$ (solid lines) with the analytical approximation (5.7) (dash-dotted). Note that the approximation improves with increasing m, as expected.

5.2 Branches with nonzero energy

For $\alpha \to \infty$ the behavior of branches of solutions with nonzero energy is little different from those with zero energy, as can be seen from the way ρ in (1.14) depends on α and E. However, for $\alpha = O(1)$ or $O(\varepsilon)$, and ε small there are important differences. It makes a difference whether $E > 0$ or $E < 0$. In both cases, branches can no longer bifurcate from the trivial solution because that solution has zero energy. Since our multi-scale analysis

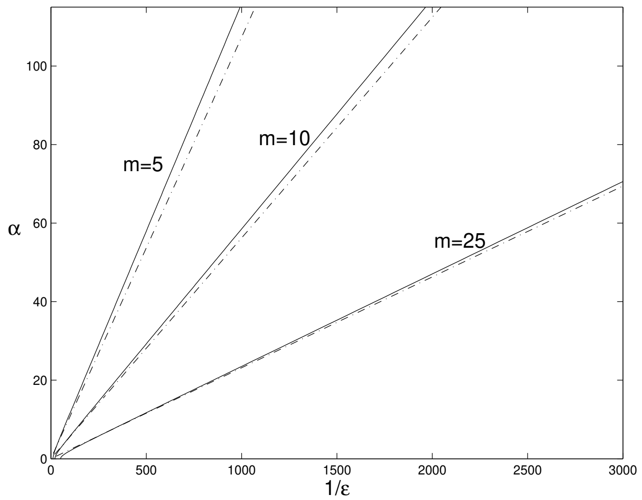

Figure 6: Bifurcation curves $\mathcal{C}_m$: numerical (solid) and asymptotic (dash-dot); cf (5.7)

is valid in this regime of small ε and $\alpha = O(1)$, it offers an insight into the way solution branches change when $E \neq 0$.

(i) If $E > 0$, the energy identity (1.8), implies that

$$\frac{1}{2}\alpha^2 + \frac{\gamma}{4}\alpha^4 \geq E > 0,$$

so that α cannot drop below a certain level, $\alpha^*(E)$ determined by the equation

$$\frac{1}{2}(\alpha^*)^2 + \frac{\gamma}{4}(\alpha^*)^4 = E.$$

In Figure 7, we show how two pairs of branches, one for $m = 7$ and one for $m = 8$, descend from large values of α. In each pair, $u''(0) < 0$ along one branch and $u''(0) > 0$ along the other, and they connect at the level α^*. The branches are computed numerically ($*$'s) as well as by the multi-scale method of this paper (solid lines).

Figure 8 shows two solutions corresponding to values on the two branches for $1/\varepsilon = 40$, $m = 8$, and $E = 5$, that is, for β both positive and negative. Notice that $u'(L) < 0$ for both solutions, as is consistent with the discussion at the beginning of this section. Then for $\beta < 0$ there are $2m + 1$ laps in a half-period, while for $\beta > 0$ the number of laps is reduced.

(ii) If $E < 0$ there is no uniform barrier as in the previous case. Instead, we have the following bound. Suppose that $\alpha = M$. Then $u''(0) < 0$, and it follows that $B(0) \geq 0$. Therefore, $0 \leq \varepsilon\rho \leq \alpha$. This implies that

$$\alpha \geq \varepsilon\sqrt{\alpha^2 + \frac{\gamma}{2}\alpha^4 + 2|E|} \geq \varepsilon\sqrt{2|E|}.$$

Note that if we put $B(0) = 0$, and hence $B(x) = 0$ for all $x \geq 0$, our asymptotics yields the following branch of 1-lap periodic solutions:

$$u(x) = \varepsilon\sqrt{2|E|}\,\cos\Big(\frac{x}{\varepsilon}\Big) + O(\varepsilon^3) \qquad \text{as} \quad \varepsilon \to 0.$$

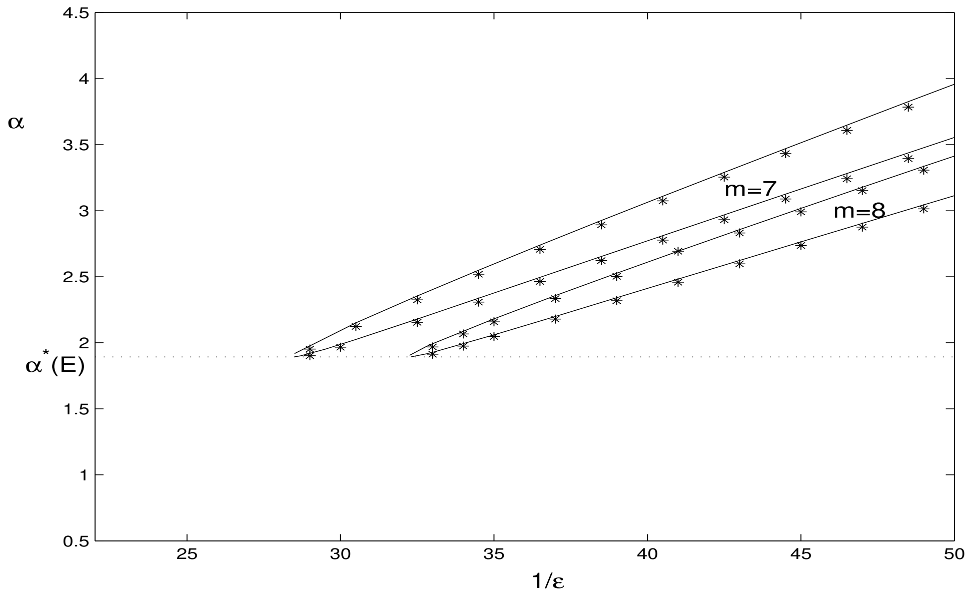

Figure 7: Solution branches for $m = 7$ and $m = 8$ when $E = +5$

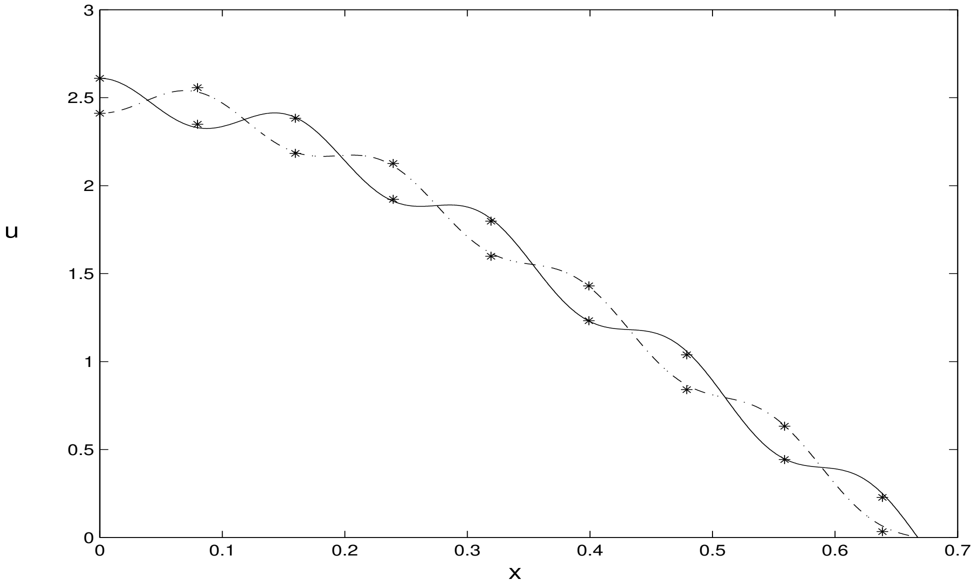

Figure 8: Asymptotic approximations to the solutions for $\beta > 0$ (dashed-dotted) and $\beta < 0$ (solid) for $m = 8$, $E = 5$, and $\varepsilon^{-1} = 40$. The $*$'s are the numerical solution.

In Figure 9 we show how branches of $n = 2m + 1$-lap solutions, with $m = 0,\ 1,\ 2,\ 3,\ 4$ and $m = 5$ descend from large values of α. The solid lines are computed numerically and the dash-dotted lines are computed using the multi-scale asymptotics. Plainly for m small the asymptotic formula are not very accurate, but for $m = 3$ and above they are already surprisingly close to the numerically computed curves. We see that the branches for $m = 1, 2, 3, 4$ and 5 approach the branch for $m = 0$ which curls around and tends to infinity along the dotted curve along which $\alpha = \varepsilon\sqrt{-2E}$.

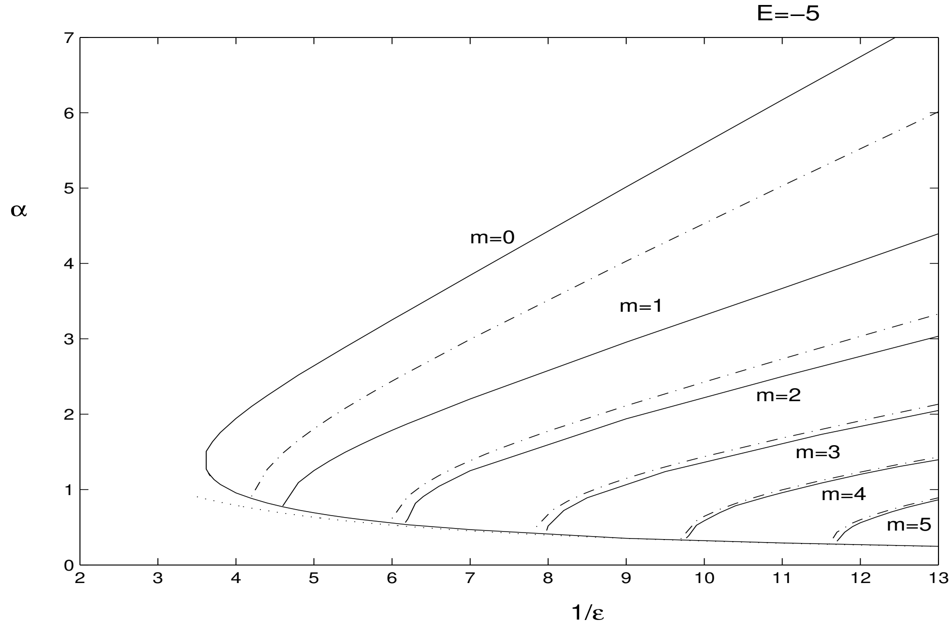

Figure 9: Solution branches for $m = 1,\ 2,\ 3,\ 4$ and 5 bifurcating from the branch for $m = 0$ when $E = -5$

In this context, it is interesting to mention a numerical rendering of branches of stationary solutions of the Swift-Hohenberg equation shown in Figure 9.3.5 of [14]. Solutions on these branches satisfy the equation

$$u^{iv} + 2u'' + (1 - \kappa)u + u^3 = 0, \qquad \kappa > 0,$$

and have energy $E = -0.005$. By an appropriate transformation, the interval $0 < \kappa < 1$ maps onto $0 < \varepsilon < \frac{1}{2}$, in such a manner that $\kappa \to 1$ corresponds to $\varepsilon \to 0$ and $\kappa \to 0$ corresponds to $\varepsilon \to \frac{1}{2}$. We see that the branch of 1-lap solutions intersects the line $\kappa = 1$ twice, once for M large, and once for M small, and that several branches bifurcate from the bottom part of the branch.

In Figure 10 we show graphs of the asymptotic approximations to solutions on the branch for $m = 3$ in Figure 9 in order to illustrate how branches for $m > 0$ connect with the branch $m = 0$ at the bottom. We give three solution graphs for decreasing values of ε^{-1}: for $\varepsilon^{-1} = 11$ ($*$'s), for $\varepsilon^{-1} = 8.1$ (solid), and for $\varepsilon^{-1} = 7.9$ (dash- dotted). We see that as ε^{-1} decreases, the high frequency oscillation dominates the baseline solution $B(x)$, and $B(x)$ tends to zero as the branch approaches the intersection with the bottom branch. For values of α where $B(x) \neq 0$, we have $L = \varepsilon(2m+1)\pi/2$. However, at the point where the branch for $m = 3$ hits the bottom branch and $B(x)$ first vanishes, which happens here at a non-trivial value of $\alpha \sim \varepsilon\sqrt{2|E|}$, the solution is given solely by $u \sim A\cos(x/\varepsilon)$, so that the definition of L implies that $L = \varepsilon\pi/2$. That is, the branch of solutions corresponding to a multi-bump solution with n laps in a half period collapses to a periodic solution, which has 1 lap in a half period. For example, in Figure 11, notice that when $\varepsilon^{-1} = 7.9$, the solution is nearly $A\cos(x/\varepsilon)$.

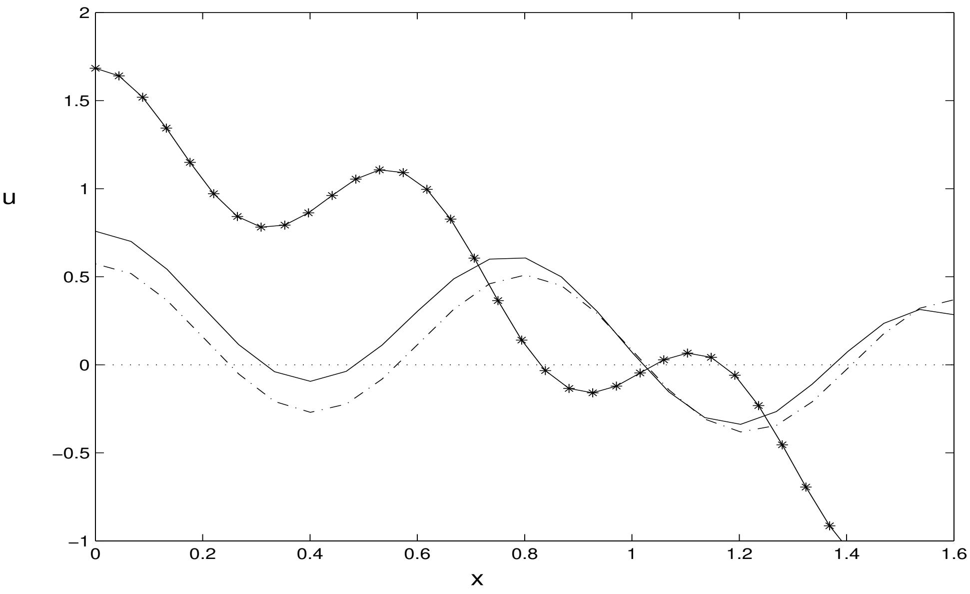

Figure 10: Asymptotic approximations to solutions along the branch $m = 3$ in Figure 9
.

5.3 Asymptotic behavior of the exponent ν

As noted in the Introduction, the branches in Figures 5 and 6 appear to be asymptotically linear, but in fact the exponent ν in the relationship $\alpha = \varepsilon^{-\nu}$ is well below unity for the values of ε shown.In this subsection we give an asymptotic expression for ν which illustrates that ν approaches unity logarithmically as ε decreases.

To determine the asymptotic behavior of the exponent ν as a function of ε, we combine the expression (5.5) for $L(\alpha)$ together with (3.3)

$$L(\alpha) = \varepsilon(2m+1)\frac{\pi}{2} = \frac{\sqrt{2}}{\alpha}\{\mathcal{J} + O(\delta) + O(\alpha^{-2})\}. \qquad m = 1, 2, 3, \ldots. \tag{5.8}$$

Then, using

$$\alpha = \varepsilon^{-\nu}$$

and taking logarithms yields

$$\nu \;=\; 1 - \frac{B_m}{\log\left(\frac{1}{\varepsilon}\right)} + O(\varepsilon^{2\nu}), \tag{5.9}$$

$$B_m \;=\; \log\Big((2m+1)\frac{\pi}{2K}\Big), \qquad K = \frac{\sqrt{2\pi}}{4}\,\frac{\Gamma(1/4)}{\Gamma(3/4)}. \tag{5.10}$$

In Figure 11 we compare (5.9) (dash-dotted line) with the exponent obtained from the numerical solution of (1.1) (circles). Again, the approximation improves with increasing m and decreasing ε.

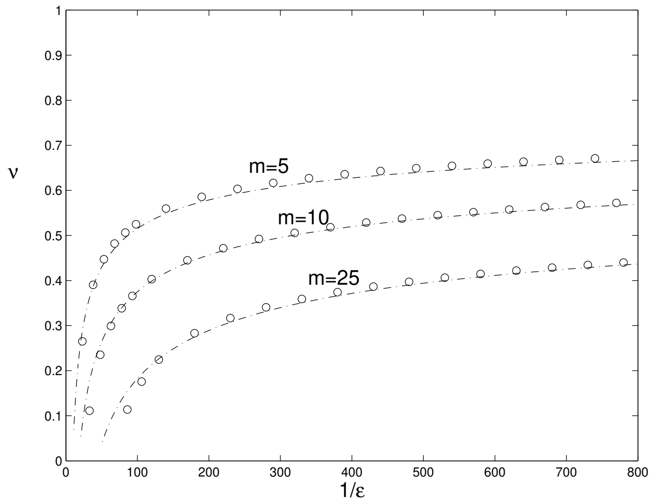

Figure 11: Graphs of ν versus ε^{-1} along the bifurcation branches C_m in Figure 6

A Appendix

Here we give the full expansion for the case $\alpha = O(1)$ (all values of E). As we show below, the general expansion allows for the high-frequency oscillations to be of the same or lower order as the baseline solution. Furthermore, other modes in the high-frequency periodic solution must be included in the uniform asymptotic expansion. Recall that in the case discussed in Section 3, we assumed that $E = O(1)$, which resulted in high-frequency oscillations which were of lower order compared with the baseline solution. The expansion which we show here is necessary for large values of E as considered in Section 4. For $E = O(1)$ the results shown below reduce to those given in Section 3.

We write $u(x)$ as in (3.4)-(3.6) and collect the coefficients of equal powers of ε^j, for $j = -2, -1, \ldots$. We first consider the $O(\varepsilon^{-2})$ equation.

$$O(\varepsilon^{-2}) \quad : \qquad U_{0\xi\xi\xi\xi} + U_{0\xi\xi} = 0, \tag{A.1}$$

and we conclude that U_0 has the form

$$U_0(x,\xi) = A_0(x)\cos(\xi) + C_0(x)\sin(\xi), \qquad \xi = \frac{x}{\varepsilon}. \tag{A.2}$$

Here we have used the symmetry conditions to eliminate terms which are linear in ξ, and absorbed terms which are functions of x only into $B(x)$. This leading order result suggests that a convenient form for the multi-scale expansion of U is

$$\begin{aligned} U(x,\xi) &= A(x)\cos(\lambda\xi) + C(x)\sin(\lambda\xi) + \varepsilon^2 D_2(x)\cos(2\lambda\xi) + \varepsilon^2 F_2\sin(2\lambda\xi) \\ &\quad + \varepsilon^3 G_2\cos(3\lambda\xi) + \varepsilon^2 H_2\sin(3\lambda\xi) + \ldots \\ A(x) &= A_0(x) + \varepsilon A_1(x) + \varepsilon^2 A_2(x) + \ldots \\ C(x) &= C_0(x) + \varepsilon C_1(x) + \varepsilon^2 C_2(x) + \ldots \\ \lambda &= \lambda_0 + \varepsilon\lambda_1 + \ldots \end{aligned} \tag{A.3}$$

Note that we have included higher order terms involving high-frequency modes of the form $\cos(j\lambda\xi)$ and $\sin(j\lambda\xi)$ for $j = 2, 3, \ldots$. We see below that these terms are necessary, because of the nonlinearity.

For later reference, we write the boundary conditions in terms of the expansions, keeping terms up to $O(1)$. At the origin, $x = 0$, we obtain

$$B'(0) + A'(0) + \frac{\lambda}{\varepsilon}C(0) = 0, \tag{A.4}$$

$$B'''(0) - \frac{\lambda^3}{\varepsilon^3}C(0) - \frac{\lambda^3}{\varepsilon}\{8F(0) + 27H(0)\} - 3\frac{\lambda^2}{\varepsilon^2}A'(0) \\ -3\lambda^2\{4D'(0) + 9G'(0)\} + \frac{\lambda}{\varepsilon}C''(0) + A'''(0) = 0, \tag{A.5}$$

and at the first zero, $x = L$, where $u'' = 0$, we have

$$B(L) + A(L)\cos\Big(\frac{\lambda L}{\varepsilon}\Big) + C(L)\sin\Big(\frac{\lambda L}{\varepsilon}\Big) = 0 \tag{A.6}$$

$$B''(L) - \frac{\lambda^2}{\varepsilon^2}\left[A(L)\cos\Big(\frac{\lambda L}{\varepsilon}\Big) + C(L)\sin\Big(\frac{\lambda L}{\varepsilon}\Big)\right] \\ -\frac{\lambda}{\varepsilon}\left[A'(L)\sin\Big(\frac{\lambda L}{\varepsilon}\Big) - C'(L)\cos\Big(\frac{\lambda L}{\varepsilon}\Big)\right] \\ +\left[A''(L)\cos\Big(\frac{\lambda L}{\varepsilon}\Big) + C''(L)\sin\Big(\frac{\lambda L}{\varepsilon}\Big)\right] = 0. \tag{A.7}$$

The analysis proceeds by substituting the expansions for A, B, C and λ, using Taylor series for the sine and the cosine about $\varepsilon = 0$, and collecting like powers of ε to obtain equations for A_j, B_j, C_j, D_j, F_j, G_j, H_j and λ_j. The leading order equation (A.1) is then

$$O(\varepsilon^{-2}): \qquad (\lambda_0^4 - \lambda_0^2)\left[A_0\cos\left(\frac{\lambda x}{\varepsilon}\right) + C_0\sin\left(\frac{\lambda x}{\varepsilon}\right)\right] = 0, \tag{A.8}$$

which implies that $\lambda_0 = 1$. Using $\lambda_0 = 1$, the $O(\varepsilon^{-1})$ equation then yields

$$\lambda_1\left[A_0\cos\left(\frac{\lambda x}{\varepsilon}\right) + C_0\sin\left(\frac{\lambda x}{\varepsilon}\right)\right] + A_0'(x)\sin\left(\frac{\lambda x}{\varepsilon}\right) - C_0'(x)\cos\left(\frac{\lambda x}{\varepsilon}\right) = 0, \tag{A.9}$$

from which we conclude that

$$\lambda_1 A_0 = C_0'(x) \qquad \text{and} \qquad \lambda_1 C_0 = -A_0'(x). \tag{A.10}$$

Combining these equations with the leading order terms in the boundary conditions,

$$O(\varepsilon^{-3}): \qquad C_0(0) = 0, \tag{A.11}$$

$$O(\varepsilon^{-2}): \qquad C_1(0) + 3A_0'(0) = 0, \\ A_0(L)\cos\left(\frac{\lambda L}{\varepsilon}\right) + C_0(L)\sin\left(\frac{\lambda L}{\varepsilon}\right) = 0, \tag{A.12}$$

we conclude that

$$A_0(x) = \rho_0\cos(\lambda_1 x) \qquad \text{and} \qquad C_0(x) = \rho_0\sin(\lambda_1 x), \tag{A.13}$$

where ρ_0 is an as yet undetermined constant, and

$$C_1(0) = 0. \tag{A.14}$$

As in Section 3, λ_1 cancels from the expression for U_0. We set $\lambda_1 = 0$, since it plays no role in the solution. It follows that

$$A_0(x) \equiv \rho_0 \qquad \text{and} \qquad C_0(x) \equiv 0. \tag{A.15}$$

The $O(\varepsilon^{-2})$ condition at $x = L$ yields

$$\cos\left(\frac{L}{\varepsilon}\right) = 0 \qquad \Longrightarrow \qquad \frac{L}{\varepsilon} = (2m+1)\frac{\pi}{2} \quad \text{for } m \text{ an integer.} \tag{A.16}$$

Next, we consider the $O(1)$ equation,

$$\begin{aligned} B_0''(x) + B_0(x) + \gamma B_0^3(x) + \frac{3}{2}\gamma B_0(x)\rho_0^2\left[1 + \cos\left(\frac{2\lambda x}{\varepsilon}\right)\right] = \\ +\left\{2C_1'(x) - \rho_0(1+2\lambda_2)\right\}\cos\left(\frac{\lambda x}{\varepsilon}\right) \\ -3\gamma B_0^2(x)\rho_0\cos\left(\frac{\lambda x}{\varepsilon}\right) - \gamma\rho_0^3\left[\frac{3}{4}\cos\left(\frac{\lambda x}{\varepsilon}\right) + \frac{1}{4}\cos\left(\frac{3\lambda x}{\varepsilon}\right)\right] \\ -12\left[D_2\cos\left(\frac{2\lambda x}{\varepsilon}\right) + F_2\sin\left(\frac{2\lambda x}{\varepsilon}\right)\right] - 72\left[G_2\cos\left(\frac{3\lambda x}{\varepsilon}\right) + H_2\sin\left(\frac{3\lambda x}{\varepsilon}\right)\right]. \end{aligned} \tag{A.17}$$

Using the orthogonality of the functions $\cos(j\lambda x/\varepsilon)$ and $\sin(j\lambda x/\varepsilon)$ for $j = 0, 1, 2\ldots$ on the interval $[0, 4L]$ we obtain the following equations:

$$\begin{aligned} & B_0''(x) + \left(1 + \frac{3}{2}\gamma\rho_0^2\right)B_0(x) + \gamma B_0^3(x) = 0, \\ & C_1'(x) = \rho_0\left[\frac{1}{2} + \lambda_2 + \frac{3}{8}\gamma\rho_0^2 + \frac{3}{2}\gamma B_0^2(x)\right], \\ & A_1'(x) = 0, \\ & 12D_2(x) = -\frac{3}{2}\gamma\rho_0^2 B_0(x), \\ & 72G_2(x) = -\frac{1}{4}\gamma\rho_0^3, \\ & F_2(x) = 0, \quad H_2(x) = 0. \end{aligned} \tag{A.18}$$

Together with the $O(\varepsilon^{-1})$ contributions to the boundary conditions:

$$\begin{aligned} & C_0(0) = 0, \\ & C_2(0) + 3A_1'(0) + 8F_2(0) + 27H_2(0) = 0, \\ & A_1(L)\sin\left(\frac{\lambda L}{\varepsilon}\right) + C_1(L)\cos\left(\frac{\lambda L}{\varepsilon}\right) = 0, \end{aligned} \tag{A.19}$$

we conclude that $A_1'(0) = D_2'(0) = G_2'(0) = C_2(0) = 0$.

Next we consider the $O(1)$ contributions to the boundary conditions. They are

$$\begin{aligned} & B_0'(0) = 0, \\ & B_0'''(0) - C_3(0) - 3A_2'(0) + C_1''(0) - 8F_3(0) - 27H_3(0) = 0 \\ & B_0(L) = 0 \\ & A_2(L)\cos\left(\frac{\lambda L}{\varepsilon}\right) + C_2(L)\sin\left(\frac{\lambda L}{\varepsilon}\right) - A_1'(L)\sin\left(\frac{\lambda L}{\varepsilon}\right) + C_1'(L)\cos\left(\frac{\lambda L}{\varepsilon}\right) = 0, \end{aligned} \tag{A.20}$$

where we have used the fact that $A_0''(L)\cos(\lambda L/\varepsilon) + C_0''(L)\sin(\lambda L/\varepsilon) = 0$. Under certain continuity assumptions about $B_0(x)$ at $x = 0$ and $x = L$, we also have

$$B_0''(L) = 0 \qquad \text{and} \qquad B_0'''(0) = 0. \tag{A.21}$$

Therefore, $B_0(x)$ solves the two-point boundary value problem

$$\begin{cases} B_0'' + KB_0 + \gamma B_0^3 = 0, & 0 < x < L, \qquad K = 1 + \dfrac{3}{2}\gamma\rho_0^2 \\ B_0'(0) = 0, \quad B_0(L) = 0. \end{cases} \tag{A.22}$$

The condition (A.16) for L in terms of ε then results in the specification of $B_0(0)$ through the solution of (A.22), i.e. given ε there is a sequence of solutions $B_{0,m}$ for m satisfying (A.16).

At this point we have the leading order asymptotic approximation

$$u(x) \sim \rho_0 \cos\left(\frac{x}{\varepsilon}\right) + B(x). \tag{A.23}$$

The values of ρ_0 and $B_0(0)$ are determined from the initial conditions (1.6) as shown in Sections 3 and 4.

It is possible to obtain higher order contributions to this approximation. For example, to obtain the next order contribution to the high-frequency oscillation, we solve the equations for $A_1(x)$ and $C_1(x)$ in (A.18). This yields

$$A_1(x) = \rho_1, \tag{A.24}$$

$$C_1(x) = \rho_0 \int_0^x \left\{\frac{1}{2} + \lambda_2 + \frac{3}{2}B_0^2(x) + \frac{3}{8}\rho_0^2\right\} dx. \tag{A.25}$$

A typical solvability condition used to determine λ_2 is

$$\int_0^L \left\{1 + \lambda_2 + \frac{3}{2}B_0^2 + \frac{3}{8}\rho_0^2\right\} dx = 0. \tag{A.26}$$

This solvability condition leads to solutions for C_1 that vanish at $x = L$.

To obtain the next order correction to the baseline solution $\epsilon B_1(x)$, we have to solve the $O(\varepsilon)$ equation. In Section 3 we showed that for $E = O(1)$ it is necessary to include $B_1(x)$ in the leading order approximation of u, since the high-frequency oscillations are also of $O(\varepsilon)$. In that case the equation for $B_1(x)$ is

$$\begin{aligned} O(\varepsilon): \quad & B_1''(x) + B_1(x) + 3\gamma B_1(x)B_0^2(x) = \\ & -(1 + 2\lambda_2)A_1\cos(\lambda\xi) - 3\gamma B_0^2\rho_0\cos(\lambda\xi), \end{aligned} \tag{A.27}$$

and the corresponding boundary conditions at $O(\varepsilon)$ are

$$\begin{cases} B_1'(0) = 0, \quad B_1(L) = 0, \\ B_1'''(0) - C_4(0) - 3A_3'(0) + C_2''(0) = 0, \\ A_3(L)\cos\left(\dfrac{\lambda L}{\varepsilon}\right) + C_3(L)\sin\left(\dfrac{\lambda L}{\varepsilon}\right) - A_2'(L)\sin\left(\dfrac{\lambda L}{\varepsilon}\right) + C_2'(L)\cos\left(\dfrac{\lambda L}{\varepsilon}\right) = 0. \end{cases}$$

We focus on the first two boundary conditions in order to determine $B_1(x)$. Once again treating ξ and x as independent variables, we have the following equation for the correction to the baseline solution B_1

$$\begin{cases} B_1''(x) + \{1 + 3\gamma B_0^2(x)\}B_1(x) = 0, \\ B_1'(0) = 0 \quad \text{and} \quad B_1(L) = 0. \end{cases} \tag{A.28}$$

The solution is

$$B_1(x) = B_0'(x)\left(c_1 + c_2 \int^x \{B_0'(s)\}^{-2}\, ds\right), \tag{A.29}$$

in which c_1 and c_2 are constants which we determine from the boundary conditions. Because $B_1'(0) = 0$ and $B_0'(0) = 0$ we find that $c_2 = 0$. This means that $B_1(L) = c_1 B_0'(L)$. Since $B_0'(L) \neq 0$ this implies that $c_1 = 0$. Therefore we conclude that $B_1(x) = 0$.

We conclude that if $E = O(1)$ as $\varepsilon \to 0$, then

$$B(x) = B_0(x) + O(\varepsilon^2) \qquad \text{as} \quad \varepsilon \to 0,$$

where $B_0(x)$ is the solution of Problem (3.2).

B Appendix

In this appendix we prove an oscillation result about the function $\tilde{u}$ which is composed of the principal two terms in the expansion (3.1) for $u(x)$:

$$\tilde{u}(x) = B_0(x) + \frac{\rho}{\varepsilon}\cos\Big(\frac{x}{\varepsilon}\Big), \tag{B.1}$$

where

$$\rho = \sqrt{\alpha^2 + \frac{1}{2}\alpha^4 - 2E}.$$

Note that $\tilde{u}''(0) < 0$ for ε small enough. An analogous analysis can be given when in (B.1) the plus sign is replaced by a minus sign and $\tilde{u}''(0) > 0$ for small ε. We recall that

$$x_k = (4k+1)\frac{\pi}{2}\varepsilon \qquad \text{and} \qquad y_k = (4k+3)\frac{\pi}{2}\varepsilon, \qquad k = 0, 1, 2, \ldots.$$

Lemma B.1 *For every ε small enough, $\tilde{u}'$ has one zero on (x_k, y_k) and one zero on (y_k, x_{k+1}).*

Proof. Because $B_0'' < 0$ and $\big(\cos(\frac{x}{\varepsilon})\big)'' > 0$ on (x_k, y_k), it follows that

$$\tilde{u}''(x) = B_0''(x) - \frac{\rho}{\varepsilon}\cos\Big(\frac{x}{\varepsilon}\Big) < 0 \qquad \text{for} \qquad x_k < x < y_k, \tag{B.2}$$

so that $\tilde{u}'$ cannot have more than one zero on (x_k, y_k). Thus it remains to consider the interval (y_k, x_{k+1}).

Let us assume that $\tilde{u}'$ has more than one zero on (y_k, x_{k+1}). Then, because $u'(y_k) > 0$, and $\tilde{u}'(x_{k+1}) < 0$, it follows that $\tilde{u}'$ has at least three zeros on (y_k, x_{k+1}), where two zeros may coincide.

Suppose that there are three zeros, z_1, z_2 and z_3, of $\tilde{u}'$ where $\tilde{u}'' \neq 0$, numbered so that $z_1 < z_2 < z_3$. Then there exist two zeros of $\tilde{u}''$, say $x = a$ and $x = b$, such that

$$y_k < z_1 < a < z_2 < b < z_3 < x_{k+1}. \tag{B.3}$$

Integrating u''' over (a, b) we find that

$$\cos\Big(\frac{b}{\varepsilon}\Big) - \cos\Big(\frac{a}{\varepsilon}\Big) = \frac{\varepsilon}{\rho} B_0'''(\theta)(b - a), \tag{B.4}$$

in which θ is some intermediate point in the interval (a, b). For convenience we write

$$a = y_k + \alpha\varepsilon, \qquad b = y_k + \beta\varepsilon \qquad \text{and} \qquad z_j = y_k + \zeta_j\varepsilon \quad (j = 1, 2, 3),$$

where α, β, $\zeta_j \in (0, \pi)$. Then (B.4) becomes

$$-\sin(\beta) + \sin(\alpha) = \frac{\varepsilon^2}{\rho} B_0'''(\theta)(\beta - \alpha). \tag{B.5}$$

Plainly, the left hand side of (B.5) must tend to zero as $\varepsilon \to 0$. There are several ways how this can happen.

(i) $\alpha \to 0$ or $\alpha \to \pi$ and $\beta \to 0$ or $\beta \to \pi$. In that case either $z_1 - y_k = o(\varepsilon)$ or $z_3 - x_{k+1} = o(\varepsilon)$, or both. This is impossible, because we know that $\tilde{u}' \neq 0$ at y_k and at x_{k+1}.

(ii) $\beta - \alpha \to 0$. Then we deduce from (B.5) that

$$\cos(\alpha) = O(\varepsilon^2) \qquad \text{as} \qquad \varepsilon \to 0,$$

so that $\alpha \to \frac{\pi}{2}$ and $\beta \to \frac{\pi}{2}$, as well as $\zeta_2 \to \frac{\pi}{2}$. Therefore

$$\tilde{u}'(z_2) \sim B_0'\Big((4k + 4)\frac{\pi}{2}\Big) < 0 \qquad \text{as} \qquad \varepsilon \to 0,$$

which means that $\limsup_{\varepsilon \to 0} \tilde{u}'(z_2) < 0$. But this is impossible, since $\tilde{u}'(z_2) = 0$.

We conclude that $\tilde{u}'$ cannot have more than one nondegenerate zero on (y_k, x_{k+1}).

Finally, suppose that there exists a sequence $\{\varepsilon_n\}$ tending to zero as $n \to \infty$, such that for each $n \geq 1$ there exists a degenerate zero $z_n \in (y_k, x_{k+1})$ of $\tilde{u}'$, i.e.

$$\tilde{u}'(z_n) = 0 \qquad \text{and} \qquad \tilde{u}''(z_n) = 0 \qquad \text{for} \qquad n \geq 1.$$

Put $z_n = y_k + \zeta_n\varepsilon$. Then, since $\tilde{u}''(z_n) = 0$ for all $n \geq 1$, it follows from (B.2) that $\zeta_n \to \frac{\pi}{2}$ as $n \to \infty$. We now arrive at a contradiction following the argument used before.

This completes the proof of Lemma B.1.

We conclude that $\tilde{u}(x)$ has precisely $n = 2m + 1$ monotone segments on the interval $(0, 2L)$, irrespective of whether m is even or odd.

Acknowledgements

The first author would like to acknowledge support through NSF-DMS 0072311 and an NSERC Discovery Grant. The second author is grateful for the hospitality enjoyed at Boston University, whilst this paper was completed.

References

[1] Abramowitz, M. & I. Stegun, *Handbook of mathematical functions*, Dover Publications, New York, 1970.

[2] Angenent, S.B., J.B. van den Berg & R.C.A.M. Vandervorst, *Contact and noncontact type Hamiltonian systems generated by second order Lagrangians*, Preprint.

[3] Berg, G.J.B. van den, L.A. Peletier & W.C. Troy, *Global branches of multi bump periodic solutions of the Swift-Hohenberg equation*, Arch. Rational Mech. Anal. **158** (2001) 91-153.

[4] Budd, C.J., G.W. Hunt & R. Kuske, *Asymptotics of cellular buckling close to the Maxwell load*, Proc. Roy. Soc. London A **457** (2001), 2935-2964.

[5] Champneys, A.R., M.D. Groves & P.D. Woods, *A global characterization of gap solitary-wave solutions to a coupled KdV system*, Phys. Lett. A , **271** (2000), 178-190.

[6] Collet, P. & J.P. Eckmann, *Instabilities and fronts in extended systems*, Princeton Series in Physics, Princeton University Press, 1990.

[7] Kevorkian, J. and J.D. Cole, *Multiple Scale and Singular Perturbation Methods* Springer-Verlag, New York, 1996.

[8] C. M. Bender and S. A. Orszag, *Advanced Mathematical Methods for Scientists and Engineers* McGraw-Hill, New York, 1978.

[9] Leizarowitz, A. & V.J. Mizel, *One dimensional infinite-horizon variational problems arising in continuum mechanics*, Arch. Rational Mech. Anal. **106** (1989) 161-194.

[10] P. Manneville, *Dissipative Structures and Weak Turbulence*, Academic Press, Boston, 1990.

[11] McKenna, P.J. & W. Walter, *Nonlinear oscillations in a suspension bridge*, Arch. Rational Mech. Anal. **87** (1987) 167-177.

[12] McKenna, P.J. & W. Walter, *Traveling waves in a suspension bridge*, SIAM J. Appl. Math. **50** (1990) 703-715.

[13] Mizel, V.J., L.A. Peletier & W.C. Troy, *Periodic phases in second order materials*, Arch. Rational Mech. Anal. **145** (1998) 343-382.

[14] Peletier, L.A. & W.C. Troy, *Spatial patterns described by the Extended Fisher-Kolmogorov (EFK) equation: Periodic solutions*, SIAM J. Math Anal. **28** (1997) 1317-1353.

[15] Peletier, L.A. & W.C. Troy, *Multibump periodic travelling waves in suspension bridges*, Proc. Roy. Soc. Edinburgh. **128A** (1998) 631-659.

[16] Peletier, L.A. & W.C. Troy, *Spatial patterns: Higher order model equations in physics and mechanics*, Birkhäuser, Boston, 2001.

[17] Ramsay, J.G., *A geologist's approach to rock deformation*, In *Inaugural Lectures – Imperial College of Science, Technology and Medicine*, pp. 131-143, London, 1967.

[18] Swift, J.B., & P.C. Hohenberg, *Hydrodynamic fluctuations at the convective instability*, Phys. Rev. A **15** (1977), 319–328.